1521-0103/360/3/388–398$25.00
THE JOURNAL OF PHARMACOLOGY AND EXPERIMENTAL THERAPEUTICS

http://dx.doi.org/10.1124/jpet.116.238048
J Pharmacol Exp Ther 360:388–398, March 2017

Activation of Nrf2 Reduces UVA-Mediated MMP-1 Upregulation via MAPK/AP-1 Signaling Cascades: The Photoprotective Effects of Sulforaphane and Hispidulin[S]

Anyamanee Chaiprasongsuk, Jinaphat Lohakul, Kitipong Soontrapa, Somponnat Sampattavanich, Pravit Akarasereenont, and Uraiwan Panich

Department of Pharmacology (A.C., J.L., K.S., S.S., P.A. and U.P.) and Center of Applied Thai Traditional Medicine, Faculty of Medicine (P.A.), Siriraj Hospital, Mahidol University, Bangkok, Thailand

Received September 28, 2016; accepted December 15, 2016

ABSTRACT

UVA irradiation plays a role in premature aging of the skin through triggering oxidative stress-associated stimulation of matrix metalloproteinase-1 (MMP-1) responsible for collagen degradation, a hallmark of photoaged skin. Compounds that can activate nuclear factor E2-related factor 2 (Nrf2), a transcription factor regulating antioxidant gene expression, should therefore serve as effective antiphotoaging agents. We investigated whether genetic silencing of Nrf2 could relieve UVA-mediated MMP-1 upregulation via activation of mitogen-activated protein kinase (MAPK)/activator protein 1 (AP-1) signaling using human keratinocyte cell line (HaCaT). Antiphotoaging effects of hispidulin (HPD) and sulforaphane (SFN) were assessed on their abilities to activate Nrf2 in controlling MMP-1 and collagen expressions in association with phosphorylation of MAPKs (extracellular signal-regulated kinase, c-Jun N-terminal kinase, and p38), c-Jun, and c-Fos, using the skin of BALB/c mice subjected to repetitive UVA irradiation. Our findings suggested that depletion of Nrf2 promoted both mRNA expression and activity of MMP-1 in the UVA-irradiated HaCaT cells. Treatment of Nrf2 knocked-down HaCaT cells with MAPK inhibitors significantly suppressed UVA-induced MMP-1 and AP-1 activities. Moreover, pretreatment of the mouse skin with HPD and SFN, which could activate Nrf2, provided protective effects against UVA-mediated MMP-1 induction and collagen depletion in correlation with the decreased levels of phosphorylated MAPKs, c-Jun, and c-Fos in the mouse skin. In conclusion, Nrf2 could influence UVA-mediated MMP-1 upregulation through the MAPK/AP-1 signaling cascades. HPD and SFN may therefore represent promising antiphotoaging candidates.

Introduction

Exposure of the skin to UV radiation is the primary cause of premature skin aging, which is a multifactorial process involving various molecular pathways (Baumann, 2007; Hwang et al., 2011a; Panich et al., 2016). A hallmark of photoaged skin is characterized by the destruction of the extracellular matrix proteins including collagen through induction of matrix metalloproteinase-1 (MMP-1 or collagenase 1), subsequently leading to compromised structural integrity of the dermis (Fisher et al., 2002; Ham et al., 2013; Jung et al., 2014). Oxidative stress mediated by UVA radiation has been suggested to play a vital role in the induction of MMP-1 produced by the skin cells, including keratinocytes as well as fibroblasts (Pluemsamran et al., 2012; Ryu et al., 2014; Chaiprasongsuk et al., 2016). UVA challenge results in excessive generation of reactive oxygen species (ROS) capable of upregulating MMP-1 expression and activity in keratinocytes (Pluemsamran et al., 2012, 2013; Park et al., 2013a).

Nuclear factor E2-related factor 2 (Nrf2), the redox-sensitive transcription factor, is a master regulator of the cellular antioxidant defense against environmental insults, including UV radiation. Nrf2 has been reported to play a beneficial role in protecting skin cells, including keratinocytes, fibroblasts, and melanocytes, against UV-induced oxidative damage and cellular dysfunction (Seo et al., 2011; Brugè et al., 2014; Gęgotek and Skrzydlewska, 2015). Thus, investigation of compounds targeting Nrf2-regulated antioxidant defense to combat oxidative stress could provide insight into development of a promising pharmacological approach to help delay skin photoaging. Concurrently, it has also been shown that the transcriptional regulation of MMP-1 is mediated by activation of activator protein-1 (AP-1) and its upstream mitogen-activated

This work was supported by National Research Council of Thailand graduate grant; Thailand Research Fund [Grant RSA5980066]; Siriraj Graduate Thesis Scholarship; Mahidol University Grant; Siriraj Research Fund (Grant R015831006); and Chalermphrakiat Grant, Faculty of Medicine, Siriraj Hospital, Mahidol University.
dx.doi.org/10.1124/jpet.116.238048.
[S] This article has supplemental material available at jpet.aspetjournals.org.

ABBREVIATIONS: 8-OHdG, 8-hydroxy-2′-deoxyguanosine; AP-1, activator protein 1; DMEM, Dulbecco's modified Eagle's medium; ERK, extracellular signal-regulated kinase; GCLC, glutamate cysteine ligase catalytic subunit; GST, glutathione S-transferase; H&E, Haemotoxylin and Eosin; HaCaT, human keratinocyte; HPD, hispidulin; JNK, c-Jun N-terminal kinase; MAPK, mitogen-activated protein kinase; MMP-1, matrix metalloproteinase-1; NQO1, NAD(P)H quinone oxidoreductase 1; Nrf2, nuclear factor E2-related factor 2; PBS, phosphate-buffered saline; ROS, reactive oxygen species; SFN, sulforaphane; siCtrl, nonsilencing siRNA controls; siNrf2, siRNA against Nrf2; siRNA, small-interfering RNA.

protein kinase (MAPK) signaling cascades (Kang et al., 2008). In addition, ROS-induced MAPK/AP-1 signaling was observed to be associated with the increased expression and production of MMP-1 in HaCaT keratinocytes and human dermal fibroblasts (Kim et al., 2015). Understanding how Nrf2 and the MAPK/AP1 signaling cascades interplay to influence the UV-mediated oxidative damage is essential for the development of novel photoprotective treatment.

Plant-derived phytochemicals targeting Nrf2 have been suggested as a promising pharmacological strategy for skin photoprotection (Liu et al., 2011; Seo et al., 2011; Kleszczyński et al., 2013). Several in vitro and in vivo studies have revealed that the isothiocyanate sulforaphane (SFN) abundantly found in cruciferous vegetables could act as an Nrf2 inducer and provided protective effects against UV-mediated skin damage and carcinogenesis through various cellular mechanisms, including upregulation of phase II cytoprotective proteins and inhibition of inflammatory responses (Talalay et al., 2007; Wagner et al., 2010; Saw et al., 2011). In addition, previous studies have suggested that Asian medicinal herbs containing hispidulin (HPD), which have traditionally been used to treat skin problems, possessed antimelanogenic properties and ability to penetrate the skin (Thitilertdecha et al., 2014; Kwak et al., 2016). In addition, we previously reported that *Clerodendrum spp*. containing HPD as an active ingredient had abilities to inhibit UVA-induced MMP-1 activity in association with upregulation of antioxidant defense in HaCaT cells (Pluemsamran et al., 2013; Thitilertdecha et al., 2014). Herbal extracts containing HPD as a possible active ingredient were demonstrated to provide anti-inflammatory effects possibly mediated by Nrf2 signaling (Akram et al., 2015). In this study, we aimed to explore further the involvement of Nrf2 in UVA-mediated MMP-1 upregulation and collagen degeneration. In addition to confirming the role of Nrf2 signaling in controlling the UVA-mediated MMP-1 upregulation, we also aimed to assess the photoprotective effects of HPD and SFN against UVA-induced MMP-1 induction and collagen depletion specifically through regulation of MAPKs, c-Jun, and c-Fos phosphorylation.

Materials and Methods

Cell Culture and Treatment. Human keratinocyte (HaCaT) cells (Cell Lines Service, Heidelberg, Germany) were grown in high glucose (4.5 g/L) Dulbecco's modified Eagle's medium (DMEM) and Ham's F-12 (DMEM/F-12) supplemented with 10% fetal bovine serum and 1% penicillin (100 U/ml)/streptomycin (100 μg/ml). All cells were maintained at 37°C in a humidified air of 5% CO_2 (P_{CO2} = 40 Torr). HPD (6-methoxyapigenin) and SFN and all other chemicals were purchased from Sigma-Aldrich (St. Louis, MO), unless otherwise indicated. The chemical structures of HPD (Chao et al., 2015) and SFN (Boddupalli et al., 2012) were previously described.

Silencing of Nrf2 via RNA Interference. A combination of four gene-specific small-interfering RNA (siRNA) against human Nrf2 (NM_006164) was used (FlexiTube GeneSolution GS4780 for NFE2L2; Qiagen, Valencia, CA, USA; catalogue 1027416). HaCaT cells were transfected with 5 nM siRNA against Nrf2 (siNrf2) or equal molar nonsilencing siRNA controls (siCtrl; Qiagen, Valencia, CA, USA; catalogue 1022076) for 48 hours. These siRNAs were earlier complexed with liposome carrier (HiPerFect Transfection Reagent; Qiagen, Valencia, CA, USA; catalogue 301705) at 0.08 μL/ng siRNA concentration by incubating mixture for 5–10 minutes at room temperature in serum-free DMEM/F-12. All siRNAs were verified to ensure achieving functional and specific silencing by evaluating mRNA and protein levels of Nrf2 and known Nrf2 target genes, including γ-glutamate cysteine ligase catalytic subunit (GCLC) and γ-glutamate cysteine ligase modifier subunit (GCLM), glutathione S-transferase (GST), and NAD(P)H quinone oxidoreductase1 (NQO1). To evaluate response of HaCaT cells transfected with siNrf2 or siCtrl to UVA irradiation, cells were washed with phosphate-buffered saline (PBS) and then irradiated with UVA (4 J/cm^2) at 48 hours post-transfection. Cells were incubated immediately with serum-free DMEM/F-12 and harvested at 1 hour postirradiation for determination of oxidant formation, at 4 and 24 hours postirradiation for MMP-1 mRNA level and activity, respectively, and at 15 minutes postirradiation for MAPK phosphorylation and AP-1 activity. The UV intensity detected at a distance of 21 cm from UVA lamp was 1 W/cm^2 using a UV meter (hand-held UV meter; Honle UV Technology, Munchen, Germany) equipped with UVA sensor (330–400 nm). The UVA source was a xenon arc lamp (Dermalight ultrA1; Hoenle, Martinsried, Germany) with emission maximum at 360 nm.

To determine an involvement of MAPK pathway in MMP-1 and AP-1 activities, the transfected cells were pretreated with 1 μM U0126, SP600125, and SB203580, specific inhibitors of extracellular signal-regulated kinase (ERK), c-Jun N-terminal kinase (JNK), and p38, respectively, in serum-free medium for 1 hour prior to UVA irradiation.

Determination of Intracellular Oxidant Formation by Flow Cytometry. Oxidant detection is based on oxidation of nonfluorescent dichlorofluorescein by intracellular ROS to produce fluorescent 2, 7-dichlorofluorescein (DCF). After UVA irradiation, cells were washed and incubated with serum-free DMEM/F-12 for 30 minutes before being incubated with 5 μM nonfluorescent dichlorofluorescein in PBS at 37°C for 30 minutes. Stained cells were immediately analyzed by flow cytometery using a fluorescence-activated cell sorter (FACS-Calibur) at excitation/emission wavelengths of 488/535 nm. For analysis, 10,000 cells per sample were gated and applied to a histogram depicting the fluorescence intensity of 2′,7′-dichlorofluorescein diacetate (DCFDA). Data were expressed as a percentage of control (100%, nonirradiated and untransfected cells).

Western Blot Analysis of Nrf2 Nuclear Localization and Phosphorylated MAPK. Total protein, cytosolic, and nuclear extracts were prepared, and immunoblotting assay was carried out to detect nuclear localization of Nrf2 and phosphorylation of MAPK (ERK, JNK, and p38), as previously described (Chaiprasongsuk et al., 2016).

Quantitative Real-Time Reverse Transcriptase-Polymerase Chain Reaction for Measurement of mRNA Expression. Total RNA was isolated using the illustra RNAspin Mini RNA Isolation Kit (GE Healthcare, Hatfield, Hertfordshire, UK), and reverse transcription was conducted using the Improm-II reverse transcriptase (Promega, Madison, WI) under the conditions described in the kit manuals. Reactions were performed with the ABI Prism 7500 Real-Time PCR System (Applied Biosystems, Foster City, CA) using the amplification conditions, as previously reported (Chaiprasongsuk et al., 2016), and the polymerase chain reaction primers listed in Table 1. The mRNA levels were normalized by the mRNA level of glyceraldehyde-3-phosphate dehydrogenase from the same cDNA samples. For the control (nonirradiated and untransfected cells), $\Delta\Delta C_t$ equals zero and 2° equals one, so that the fold change in gene expression relative to the control equals one, by definition. For the UV-irradiated and compound-treated cells, assessment of $2^{-\Delta\Delta Ct}$ indicates the fold change in gene expression relative to the control.

Determination of MMP-1 Activity. MMP-1 activity in conditioned media collected at 24 hours following UVA irradiation was determined using gelatin zymography, as previously described (Pluemsamran et al., 2012). In brief, culture supernatants were mixed 1:1 (v/v) with nonreducing SDS sample buffer [125 mM Tris-HCl (pH 6.8), 20% glycerol, 2% SDS, 0.002% bromophenol blue] and were subjected to electrophoresis on 10% polyacrylamide gels containing 1% gelatin. Following electrophoresis, the gels were washed twice with 2.5% Triton X-100 for 30 minutes to remove SDS and to renature the MMP-1 in the gels. Renaturated gels were incubated in developing buffer for 24 hours at 37°C to induce gelatin lysis and were later

TABLE 1
Sequences (in 5′-3′ direction) of primers used in this study

Primer	Sequences	Product Size (bp)	GeneBank
Nrf2 (sense)	5′-TTCTGTTGCTCAGGTAGCCCCTCA-3′	161	NM_006164.4
Nrf2 (antisense)	5′-GTTTGGCTTCTGGACTTGG-3′		
GCLC (sense)	5′-GCTGTCTTGCAGGGAATGTT-3′	160	NM_001498.2
GCLC (antisense)	5′-ACACACCTTCCTTCCCATTG-3′		
GCLM (sense)	5′-TTGGAGTTGCACAGCTGGATT-3′	200	NM_002061.2
GCLM (antisense)	5′-TGGTTTTACCTGTGCCCACTG-3′		
GST (sense)	5′-CCTGTACCAGTCCAATACCATCCT-3′	72	NM_000852.3
GST (sense)	5′-TCCTGCTGGTCCTTCCCATA-3′		
NQO1 (sense)	5′-ATGACAAAGGACCCTTCCGGAGTAA-3′	245	NM_000903.2
NQO1 (antisense)	5′-ATTCTCCAGGCGTTTCTTCCATCCT-3′		
MMP-1 (sense)	5′-CCTCTGATGCCTCTGAGAAGA-3′	267	NM_001145938.1
MMP-1 (antisense)	5′-TCCTCCCCTTATGGATTCCT-3′		
GAPDH (sense)	5′-CCTCCAAAATCAAGTGGGGCGATG-3′	150	NM_002046.3
GAPDH (antisense)	5′-CGAACATGGGGGCATCAGCAGA-3′		

GAPDH, glyceraldehyde-3-phosphate dehydrogenase. GCLM, γ-glutamate cysteine ligase modifier subunit.

stained with 0.006% Coomassie brilliant blue G-250 (50% methanol, 10% acetic acid) for 2 hours and destained using destaining solution (50% methanol, 10% acetic acid) for 5 minutes at room temperature. Gelatinolytic activity was observed as colorless (unstained) bands. Determination of MMP-1 activity was performed by scanning the gels using a CAMAG TLC scanner (St. Gallen, Muttenz, Switzerland), and integrated density for each band was calculated using the ImageMaster software (Hoefer Pharmacia Biotech, San Francisco, CA, USA). Data were expressed as arbitrary densitometric units of MMP-1 activity per 1,000,000 cells.

Determination of AP-1 Transcriptional Activity. Transcriptional activity of AP-1 was evaluated using the Cignal Activator Protein-1 Reporter (luc) Kit (SABiosciences, Qiagen, Valencia, CA, USA). HaCaT cells were transfected with an AP-1–responsive firefly luciferase reporter plasmid and a control plasmid constitutively expressing *Renilla* luciferase (SABiosciences, Qiagen, Valencia, CA, USA) in Lipofectamine Reagent (Invitrogen), according to the manufacturer's instructions. The transfected cells were further incubated in serum-free medium and harvested at 15 minutes following UVA irradiation. The firefly and *Renilla* luciferase activities were determined using a Dual-Glo Luciferase Assay Kit (Promega) in a luminometer (FLUOstar Omega, BMG Labtech, Almendgruen, Ortenberg, Germany). Firefly luciferase activity was normalized to *Renilla* luciferase activity to account for transfection efficiency.

Animals and Treatment. BALB/c mice were obtained from National Laboratory Animal Center, Mahidol University. They were housed under controlled conditions (25 ± 2°C with a 12-hour light and 12-hour dark cycle) using an isolator caging system and water ad libitum during the experimental period.

BALB/c mice were randomized into seven groups of nine mice each, described as follows. Group I (control) did not undergo UVA irradiation or any topical treatment. Group II (sham) was topically treated with ethanol:acetone (1:1, v:v) without UVA irradiation. Group III (UVA) was irradiated with UVA at 10 J/cm^2/session three times per week for 2 weeks (a total dose of 60 J/cm^2). Group IV (sham with UVA) was topically treated with ethanol:acetone (1:1, v:v) and irradiated with UVA at 10 J/cm^2/session three times per week for 2 weeks (a total dose of 60 J/cm^2). Group V (HPD with UVA) was topically treated with 20, 60, and 200 μM/cm^2 HPD (dissolved in 20 μl ethanol:acetone 1:1, v:v) to the dorsal skin prior to UVA irradiation. Group VI (SFN with UVA) was topically treated with 0.6 μM/cm^2 SFN (dissolved in 20 μl ethanol:acetone 1:1, v:v) to the dorsal skin prior to UVA irradiation. Group VII (treatment without UVA) was topically treated with HPD at the highest dose (200 μM/cm^2) used in this study or SFN (0.6 μM/cm^2) to the dorsal skin without UVA irradiation.

Mice (4–5 weeks of age) were anesthetized by i.p. injection of ketamine/xylazine. HPD and SFN were topically applied to a 1-cm^2 area of the shaved dorsal skin 1 hour prior to each UVA irradiation (10 J/cm^2 for three times per week up to 2 weeks; the total cumulative dose was 60 J/cm^2) (Grimbaldeston et al., 2003; Sayama et al., 2010, Shimada et al., 2011). The dorsal skin flaps were then removed at different time points, as indicated in *Results*. The fresh skin tissues were embedded in Tissue-Tek OCT compound and frozen directly in liquid nitrogen. Frozen tissues were stored at −80°C until sectioning.

An inverted fluorescent microscope equipped with an inverted fluorescent microscope with camera (Ti-S Intensilight Ri1 NIS-D) (Nikon, Tokyo, Japan) was used for the imaging of Haemotoxylin and Eosin (H&E) and immunofluorescence stainings according to the inverted microscope manufacturer's instructions, which were quantified using ImageJ software (Gawronska-Kozak et al., 2016).

H&E Staining and Analysis of Skin Thickness. Cryo-cut tissue sections (8 μm) were fixed in ice-cold acetone and air dried for 30 minutes at room temperature. H&E staining was performed for histologic evaluation of skin thickness. Tissue sections were washed in distilled water for 2 minutes, incubated with hematoxylin for 4 minutes, and then washed in distilled water for 10 minutes. The slides were then incubated with eosin for 1 minute and 95% alcohol for 1 minute. The slides were dehydrated with 95% alcohol (15 seconds), two changes of absolute alcohol (15 second each), two changes of acetone (15 second each), and three changes of xylene (15 second). Stained slides were mounted in mounting medium and then covered with a coverslip for viewing with a microscope.

Immunofluorescence Analysis of Nrf2 Nuclear Translocation and Its Target Proteins (GCLC, GST, and NQO-1), Oxidative DNA Damage, MMP-1, Collagen, Phosphorylated MAPK (Phosphorylated ERK, Phosphorylated JNK, and Phosphorylated p38), and Phosphorylated AP-1 Subunit (p-c-Fos and p-c-Jun). Dorsal skin tissue samples were collected at various time points following the final UVA irradiation: 1 and 6 hours postirradiation for Nrf2 and its target proteins, respectively; 1 hour postirradiation for oxidative DNA damage; 24 hours postirradiation for MMP-1 and collagen; and 15 minutes postirradiation for phosphorylated MAPK and AP-1 subunit. Tissue sections were blocked with PBS containing 2% bovine serum albumin for 30 minutes. After removing excess blocking buffer, the slides were incubated with Nrf2 Ab (ab31163; Abcam, Cambridge, MA), GCLC (ab53179; Abcam), GST Ab (sc-459; Santa Cruz Biotechnology, Santa Cruz, CA), NQO1 Ab (ab34173; Abcam) (1:50), 8-hydroxy-2′-deoxyguanosine (8-OHdG; N45.1) Ab (ab48508; Abcam) (1:50), MMP-1 Ab (ab137332; Abcam) (1:50), collagen I (C-18) Ab (sc-8784; Santa Cruz Biotechnology) (1:50), phospho-ERK Ab p44/42 MAPK (Thr^{202}/Tyr^{204}) (4370S; Cell Signaling Technology, Beverly, MA, USA), phospho-JNK Ab (Thr^{183}/Tyr^{185}) (G9) (9255S; Cell Signaling Technology, Beverly, MA, USA), phospho-p38 Ab (Thr^{180}/Tyr^{182}) (D3F9) (4511S; Cell Signaling Technology, Beverly, MA, USA), phospho-c-Fos (Ser^{32}) Ab (D82C12) (5348; Cell Signaling Technology, Beverly, MA, USA), and phospho-c-Jun (Ser^{63}) Ab (9261; Cell Signaling Technology, Beverly, MA, USA) for 1 hour. The slides were then washed three times with a PBS solution

and incubated for 1 hour at room temperature with fluorescein isothiocyanate–conjugated secondary Ab (green) and with 4′,6′-diamidino-2-phenylindole (blue) to counterstain the nuclei for detection of nuclear Nrf2, the secondary Ab Alexa Fluor 488 goat anti-rabbit (Abcam) for detection of MMP-1, collagen, and phosphorylated protein levels.

Data Analysis. ImageJ software (National Institutes of Health, Rockville, MD) was used to quantify thickness and fluorescence intensity of each protein. For analysis of skin thickness, predefined scale bar of known distance (50 μm) was used as distance calibration (Supplemental Fig. 5A). A straight line was manually drawn perpendicularly to the epidermal layer, and the length was read off directly from the software (Supplemental Fig. 5B).

For fluorescence intensity analysis, an outline was manually drawn around area of fluorescence emission to define regions of interest. For all analysis of protein expression data, the corrected total cryosection fluorescence was calculated using the following equation: cryosection fluorescence = integrated density − (area of each region of interest × mean fluorescence of background readings) (Supplemental Fig. 6A), and the data were presented as percentage of control (Noursadeghi et al., 2008; McCloy et al., 2014). Quantitative fluorescence data from ImageJ were then imported into Microsoft Excel for generating histograms for further analysis. For analysis of Nrf2 nuclear localization, we determined Nrf2 subcellular localization based on the ratio of nuclear to cytoplasmic intensity of Nrf2. The nuclear and cytoplasmic compartment was manually drawn, as shown in Supplemental Fig. 6B. Intensity from each compartment was corrected by the background intensity.

Statistical Analysis. Data for in vitro study were reported as means ± S.D. from at least three biologic replicates ($n \geq 3$) performed on different days using freshly prepared reagents. The significance of nonirradiated controls or individual treatment groups in comparison with the UVA-irradiated groups was evaluated by independent t test (Student's; two populations) or one-way analysis of variance, followed by Tukey or Dunnett tests, where appropriate, using Prism (GraphPad Software, San Diego, CA). Data for in vivo study are reported as means ± S.D. The significance of nonirradiated controls or sham controls or individual treatment groups in comparison with the sham-irradiated mice was evaluated by independent t test (Student's; two populations) or one-way analysis of variance, followed by Tukey or Dunnett tests, where appropriate.

Results

Depletion of Nrf2 Augmented UVA-Induced MMP-1 via Modulation of MAPK/AP-1 Signaling in Keratinocyte HaCaT Cells. We previously reported that UVA caused MMP-1 upregulation through induction of oxidative stress and depletion of antioxidant defenses in HaCaT cells (Pluemsamran et al., 2012, 2013). Depletion of Nrf2 has been widely demonstrated to compromise cellular redox balance and cause susceptibility to oxidative stress in various cell types in response to various stimuli (Frohlich et al., 2008; Rushworth et al., 2011). We thus hypothesized that Nrf2 function must also underlie the UVA-induced MMP-1 upregulation. To test this, we first compared the changes of MMP-1 mRNA expression and activity between siNrf2 and siCtrl-transfected HaCaT cells. Efficiency of Nrf2 knockdown in HaCaT cells was verified by real-time reverse-transcription polymerase chain reaction and Western blot analysis, showing successful depletion of Nrf2 down to ~40% and a significant decrease of its target antioxidant genes by 48 hours following the transfection, in comparison with untransfected and siCtrl HaCaT cells (Supplemental Fig. 1). In control HaCaT cells, UVA irradiation led to a substantial induction of MMP-1 mRNA levels (Fig. 1A) and activity (Fig. 1B; Supplemental Fig. 2A) at 4 and 24 hours postirradiation, respectively. Similar results were also observed in siCtrl-transfected cells. With depletion of Nrf2, UVA-irradiated cells exhibit substantial increases of MMP-1 mRNA and activity than those in siCtrl-transfected cells, whereas nonirradiated cells did not exhibit any differences (Fig. 1, A and B; Supplemental Figs. 1 and 2A).

MAPK signaling was shown to be associated with the regulation of MMP-1 activity in HaCaT keratinocytes and human dermal fibroblasts (Kim et al., 2015), although activation of MMP-1 via MAPK/AP-1 signaling in the UVA-mediated response of keratinocytes remains unclear. In HaCaT cell line, we found that UVA irradiation significantly promotes phosphorylation of ERK, JNK, and p38 as early as 15 minutes (Supplemental Fig. 2B). To quantify the involvement of each MAPK pathway on UVA-stimulated MMP-1 activity, we measured MMP-1 activity after irradiation with UVA (4 J/cm^2) in HaCaT cells that were pre-exposed to inhibitors of ERK, JNK, or p38 signaling cascades (U0126 as a selective inhibitor of ERK, SP600125 as a selective inhibitor of JNK, and SB203580 as a selective inhibitor of p38). Inhibition of MAPK signaling cascades was found to substantially reduce MMP-1 activity in irradiated HaCaT cells (Supplemental Fig. 2C). Similar reduction level was observed from addition of individual inhibitor or all three inhibitors combined, indicating that all three signaling cascades are required for MMP-1 regulation.

We next investigated the involvement of MAPK/AP-1 signaling in the Nrf2-dependent regulation of UVA-induced MMP-1 activity. With Nrf2 depletion of HaCaT cells, inhibition of MAPK signaling cascades, either individually or all three pathways simultaneously, was observed to revert the previously observed upregulation of UVA-induced MMP-1 activity (Fig. 1A), correspondingly with the diminished AP-1 transcriptional activity (Fig. 1C). Depletion of Nrf2 also led to a marked increase in UVA-mediated MAPK phosphorylation as compared with siCtrl-transfected cells following irradiation (Fig. 1D). ROS has been shown to be associated with the activation of MAPK signaling cascades in various cell types, including the skin cells. Prior studies also showed that ROS-induced phosphorylation of ERK, JNK, and p38 could mediate UVA-induced biologic responses, including apoptosis (Gao et al., 2007; López-Camarillo et al., 2012) and MMP-1 release (Hwang et al., 2011b; López-Camarillo et al., 2012; Kammeyer and Luiten, 2015) in HaCaT cells. In this study, we observed the elevated level of ROS in Nrf2-depleted HaCaT cells as early as 15 minutes following UVA challenge (Supplemental Fig. 3). Moreover, treatment of HaCaT cells with H_2O_2 alone for 15 minutes caused a pronounced induction of phosphorylated ERK, JNK, and p38 (Fig. 1E). Collectively, these results showed that, under Nrf2 deficiency, UVA-stimulated oxidative insults promote MMP-1 upregulation via activation of MAPK/AP-1 signaling.

Activation of Nrf2 in the Mouse Epidermis by Pharmacological Agents. Our in vitro study implied that Nrf2 is required for protection against UVA-stimulated MMP-1 upregulation. We were therefore interested to examine whether activation of Nrf2 can in fact protect the skin from the UVA-mediated damage. To test this hypothesis, we assessed the photoprotective effects of two compounds, SFN, a well-recognized Nrf2 activator, as well as HPD, an

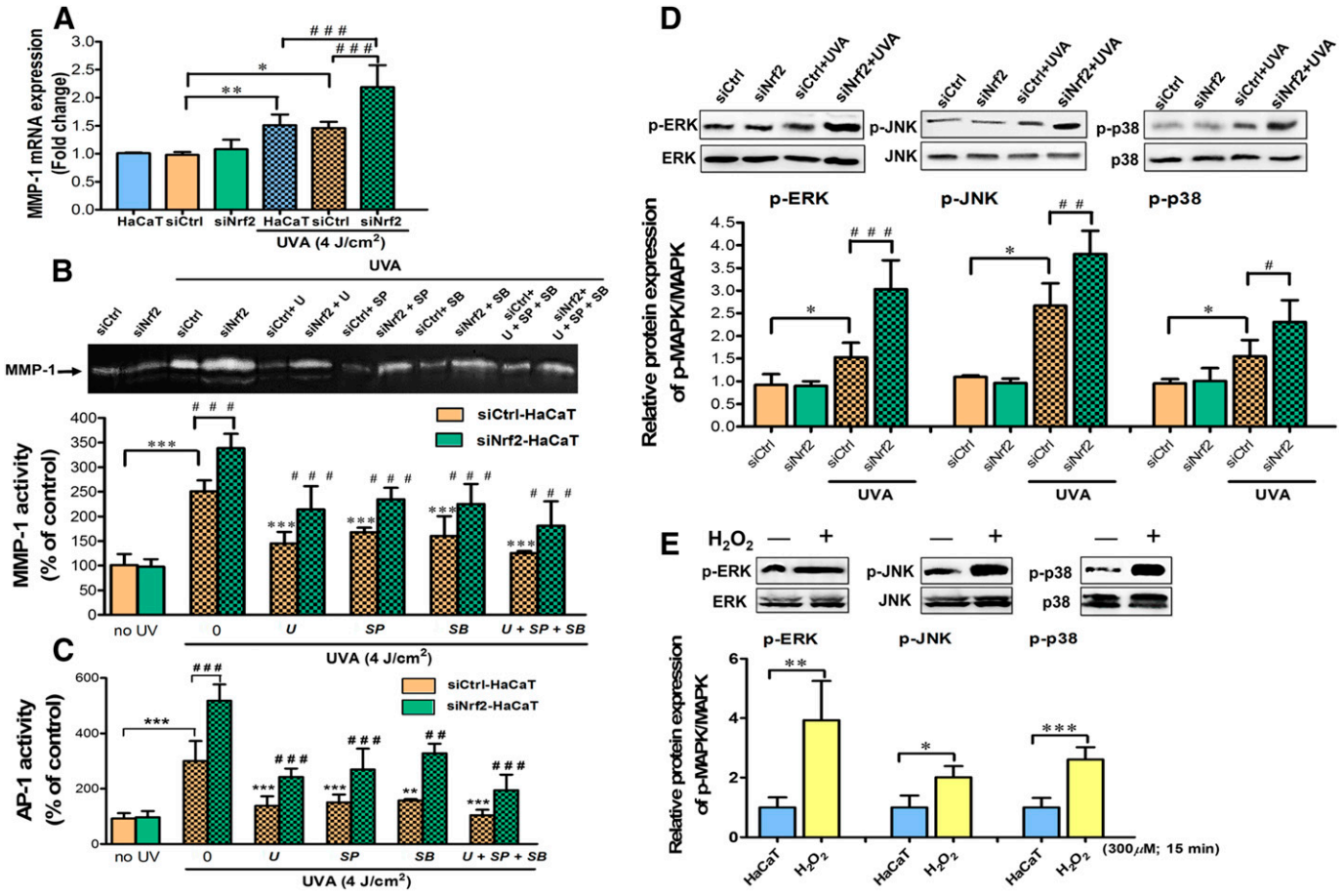

Fig. 1. Depletion of Nrf2 increased UVA-induced MMP-1 via modulation of MAPK/AP-1 signaling in keratinocyte HaCaT cells. (A) MMP-1 mRNA expression in HaCaT cells transfected with siNrf2 or siCtrl at 4 hours postirradiation. (B) UVA-stimulated MMP-1 activity under Nrf2 depletion with different MAPK inhibitors. HaCaT cells were transfected with siNrf2 or siCtrl for 48 hours and incubated with 1 μM U0126, SP600125, and SB203580 (specific inhibitor of ERK, JNK, and p38) for 1 hour prior to UVA (4 J/cm^2) irradiation. MMP-1 activity was measured in HaCaT cells transfected with siNrf2 or siCtrl at 24 hours postirradiation. (C) AP-1 activity was measured in HaCaT cells transfected with siNrf2 or siCtrl at 15 minutes postirradiation and evaluated by AP-1 luciferase assay. (D) Nrf2 depletion enhanced UVA-mediated MAPK phosphorylation. Phosphorylated MAPKs (p-ERK, p-JNK, and p-p38) were determined in HaCaT cells transfected with siNrf2 or siCtrl at 15 minutes postirradiation using Western blotting. Data were expressed as mean ± S.D. The statistical significance of differences was evaluated by one-way analysis of variance, followed by Dunnett's test. *$P <$ 0.05; **$P < 0.01$; ***$P < 0.001$ versus siCtrl-transfected cells without UVA irradiation. #$P < 0.05$; ##$P < 0.01$; ###$P < 0.001$ versus siNrf2-transfected cell-irradiated UVA. (E) Changes of MAPK activation with addition of H_2O_2. HaCaT cells were incubated with 300 μM H_2O_2 for 15 minutes and then were harvested for measurement of ERK, JNK, and p38 phosphorylation using Western blotting. *$P < 0.05$; **$P < 0.01$; ***$P < 0.001$ versus control cells without H_2O_2.

antioxidant phytochemical with high dermal permeability, in the in vivo setting. BALB/c mice were used in this study because they have been shown to preserve the expression of glycosaminoglycans in the dermis, which are critical for structural integrity of the skin similarly to that observed in the human physiology (Avci et al., 2013). We first determined the physiologic changes of Nrf2 activities and its target antioxidant genes in the mouse skin following UVA exposure. As shown in Fig. 2, A and B, UVA up to 90 J/cm^2 irradiation was found to mediate dose- and time-dependent changes of Nrf2 activity in the mouse skin. Specifically, we observed a substantial decrease of Nrf2 activity at 1 hour after the final UVA exposure, followed by a gradual increase of Nrf2 activity that got completely restored by 12 hours after UVA exposure. These findings are consistent with our results from in vitro models demonstrating the decrease of nuclear/cytosolic Nrf2 ratios in HaCaT cells (Supplemental Fig. 4) and B16F10 melanoma cell as early as 1 hour after UVA irradiation at the dose of 4 and 8 J/cm^2, respectively (Chaiprasongsuk et al., 2016). UVA-irradiated skin also showed a drastic reduction of Nrf2 target antioxidants. Expression of glutamate cysteine ligase, the rate-limiting enzyme of GSH synthesis, GST, and NQO1 in the epidermis was also observed to be lowered by 6 hours following the final UVA exposure (Fig. 3, A and B).

Next, we assessed whether pharmacological activation of Nrf2 could promote the antioxidant defense system. Specifically, HPD at the concentrations of 20, 60, and 200 μM/cm^2 and SFN at the concentrations of 0.6 μM/cm^2 were topically administered to mice 1 hour prior to UVA irradiation at 10 J/cm^2/session, three times per week for 2 weeks (total of 60 J/cm^2). Nrf2 activity (as observed by the elevated nuclear-to-cytosolic ratio) (Fig. 2, C and D) and protein levels of its target antioxidants (Fig. 3, A and B) in the epidermis of irradiated skin were observed to be significantly higher in the treated group than the sham-irradiated skin in absence of compound treatment. Interestingly, under no UVA irradiation, HPD treatment did not affect nuclear localization of Nrf2 nor levels of its target antioxidants (glutamate cysteine ligase,

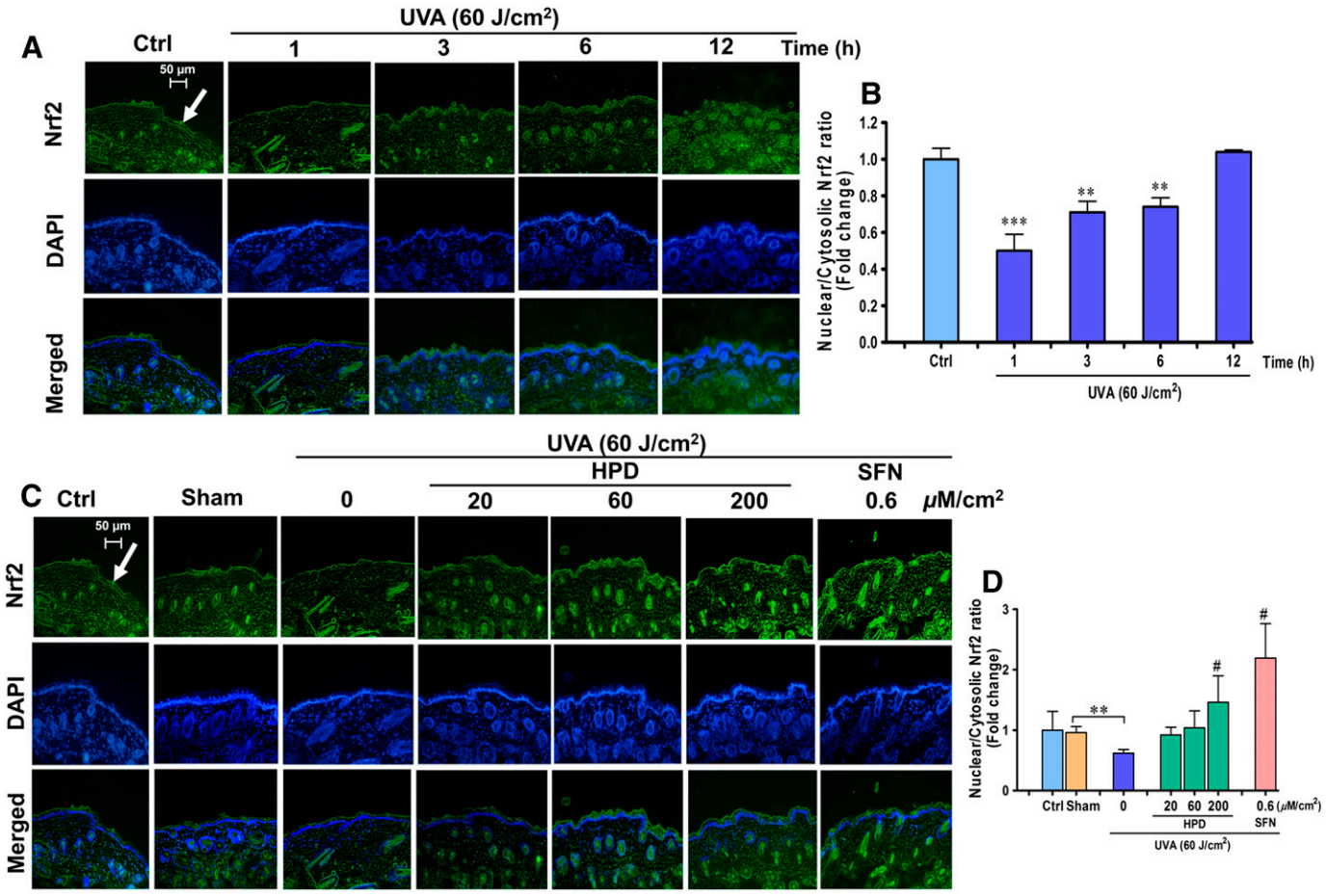

Fig. 2. Activation of Nrf2 in the epidermis by HPD in vivo. (A) Images of immunofluorescence staining for Nrf2 nuclear localization in mouse epidermis harvested at various time points after the last UVA exposure. Mice were irradiated with UVA (10 J/cm^2/session three times per week for 2 weeks; a total dose of 60 J/cm^2), and immunofluorescence was performed to determine Nrf2 nuclear translocation at 1, 3, 6, and 12 hours following the final irradiation. Fluorescein isothiocyanate–conjugated secondary antibody staining indicated location of Nrf2 (green) by anti-Nrf2 antibody. The 4′,6′-diamidino-2-phenylindole staining indicated the location of the nucleus (blue), and the merged image indicated the nuclear localization of Nrf2. (B) Levels of nuclear/cytosolic Nrf2 in mouse epidermis were quantified by ImageJ software and were expressed as mean ± S.D., $n = 9$. The statistical significance of differences between control groups and the UVA-irradiated groups was evaluated by one-way analysis of variance, followed by Dunnett's test. $^{**}P < 0.01$; $^{***}P < 0.001$ versus unirradiated control skin. (C) HPD and SFN restored Nrf2 activity of the skin under UVA irradiation. Dorsal skin was pretreated with 20, 60, and 200 μM/cm^2 HPD and 0.6 μM/cm^2 SFN for 1 hour prior to each UVA irradiation (10 J/cm^2/session three times per week for 2 weeks; a total dose of 60 J/cm^2). The skin was collected at 1 hour following the last UVA exposure. (D) Levels of nuclear/cytosolic Nrf2 modulated by topical application of HPD and SFN prior to UVA exposure were quantified by ImageJ software. Data were shown as mean ± S.D., $n = 9$. The statistical significance of differences between unirradiated sham control groups and the sham-irradiated groups was evaluated by independent Student's t test. $^{**}P < 0.01$ versus unirradiated control skin (sham). The statistical significance of differences between irradiated groups pretreated with compounds and the sham-irradiated groups was evaluated by one-way analysis of variance, followed by Dunnett's test. $\#P < 0.05$ versus the sham-irradiated groups.

GST, and NQO1), whereas SFN treatment dramatically induced the nuclear Nrf2 levels (Supplemental Fig. 7) and its target antioxidant proteins (Supplemental Fig. 8) in unirradiated (sham) skin. To assess the efficacy of Nrf2 activation to protect against UVA-mediated DNA damage, we quantified the formation of 8-OHdG, a sensitive marker of oxidative DNA damage, in the mouse epidermis at 1 hour following the final UVA exposure with cumulative doses of 60 J/cm^2. Mouse skin topically applied with HPD or SFN prior to UVA irradiation revealed a significant decrease in 8-OHdG formation in epidermal layer (Fig. 3, C and D), indicating that activation of Nrf2 can protect cells against UVA-mediated DNA damage.

Protection against UVA-Induced Connective Tissue Damage by Nrf2 Activation. Damage to dermal connective tissue that is mainly composed of type I collagen is a hallmark of photoaged skin. UVA has been suggested to induce upregulation of several MMPs, in particular MMP-1, an important enzyme responsible for collagen destruction due to oxidative stress in both keratinocytes and fibroblasts (Pluemsamran et al., 2012; Ryu et al., 2014). In our study, we confirmed that UVA exposure causes a dose-dependent upregulation of MMP-1 abundance at 24 hours after the final irradiation, following repetitive irradiation of 10 J/cm^2 UVA at a cumulative dose of 60 J/cm^2 (Supplemental Fig. 10). Type I collagen was also found to be correspondingly lowered in the dermis of UVA (60 J/cm^2)-irradiated hairless mice, whereas H&E-stained sections of skin tissues revealed thickening of the epidermal layer (Supplemental Fig. 9). With topical application of HPD or SFN 1 hour prior to each UVA irradiation, we observed a pronounced reduction in MMP-1 expression (Fig. 4, C and D), an increase of collagen levels (Fig. 4, E and F), and a marked reduction of epidermal thickness (Fig. 4, A and B), compared with sham-irradiated mice without

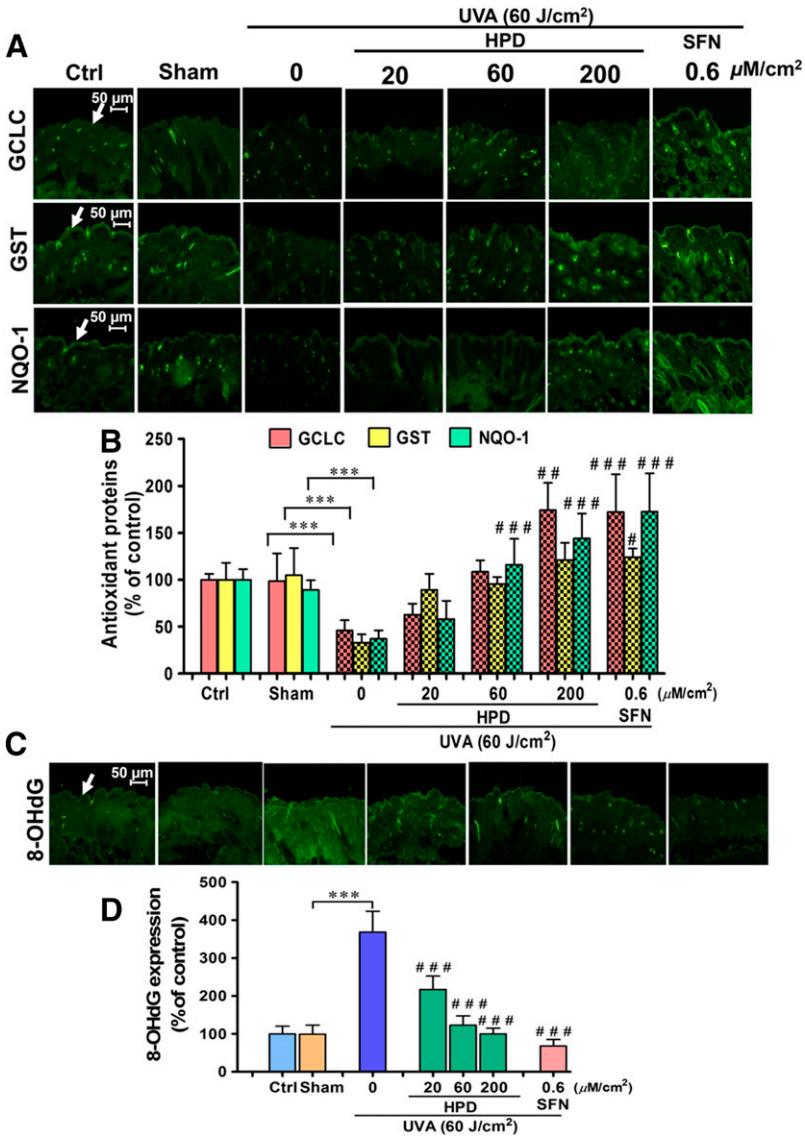

Fig. 3. HPD and SFN restored Nrf2-dependent antioxidant proteins and reduced oxidative DNA damage under UV irradiation in vivo. (A) Images of immunofluorescence staining for GCLC, GST, and NQO-1 in mouse epidermis harvested at 6 hours after the last UVA exposure. Dorsal skin was pretreated with 20, 60, and 200 μM/cm^2 HPD and 0.6 μM/cm^2 SFN for 1 hour prior to each UVA irradiation (10 J/cm^2/session three times per week for 2 weeks; a total dose of 60 J/cm^2). The skin was collected at 6 hours following the last UVA exposure. (B) Protein levels of GCLC, GST, and NQO-1 modulated by topical application of HPD and SFN prior to UVA exposure were quantified by ImageJ software. (C) Images of immunofluorescence staining for oxidative DNA damage (8-OHdG) in mouse epidermis. Dorsal skin was pretreated with 20, 60, and 200 μM/cm^2 HPD and 0.6 μM/cm^2 SFN for 1 hour prior to each UVA irradiation (10 J/cm^2/session three times per week for 2 weeks; a total dose of 60 J/cm^2). The skin was collected at 6 hours following the last UVA exposure. (D) The 8-OHdG levels modulated by topical application of HPD and SFN prior to UVA exposure were quantified by ImageJ software. Data were shown as mean ± S.D., n = 9. The statistical significance of differences between unirradiated sham control groups and the sham-irradiated groups was evaluated by independent Student's t test. ***$P < 0.001$ versus unirradiated control skin (sham). The statistical significance of differences between irradiated groups pretreated with compounds and the sham-irradiated groups was evaluated by one-way analysis of variance, followed by Dunnett's test. #$P < 0.05$; ##$P < 0.01$; ###$P < 0.001$ versus the sham-irradiated groups.

compound treatment. These results show that both test compounds can delay photoaging process, specifically those that are associated with the increase of MMP-1 and collagen degeneration.

Nrf2 Activators Promote Reduction of MMP-1 Activity via MAPK/AP-1 Signaling Cascade. The activation of MAPKs/AP-1 signaling cascades has been implicated in upregulation of MMP-1 in previous studies (Endo et al., 2009; Kook et al., 2011) and was confirmed in our in vitro model. To examine whether HPD and SFN may modulate the MMP-1 upregulation via MAPK/AP-1 signaling, we performed immunofluorescence staining to quantify impacts of topical compound treatment on the phosphorylation of ERK, JNK, and p38 as well as c-Fos and c-Jun phosphorylation (for AP-1 activation) in the epidermis and dermis of hairless mice at 15 minutes following the final UVA irradiation (a total dose of 60 J/cm^2). Our results demonstrated that topical application of HPD or SFN before UVA irradiation for 2 weeks resulted in a substantial decrease in phosphorylation of phosphorylated ERK (Fig. 5, A and B), phosphorylated JNK (Fig. 5, C and D), p38 (Fig. 5, E and F), as well as reducing phosphorylation of c-Fos (Fig. 5, G and H) and c-Jun (Fig. 5, I and J) required for AP-1 activation, in comparison with the sham-irradiated mice without compound treatment. The results therefore imply the involvement of MAPK/AP-1 pathways in the UVA-mediated upregulation of MMP-1, although future in vivo studies are still required to confirm that MAPK inhibition can indeed rescue MMP-1 upregulation following UVA irradiation of the mouse skin.

Discussion

The protective role of Nrf2 in photo-oxidative stress and damage of the skin cells, including melanocytes and keratinocytes, has been discussed (Wondrak et al., 2008; Chaiprasongsuk et al., 2016), although the molecular mechanisms by which Nrf2 protected against UVA-induced stimulation of MMP-1 accountable for collagen degradation involved in photoaging process have not been reported. Our in vitro results indicated that a partial knockdown of Nrf2 promoted UVA-mediated MMP-1 activity and mRNA in HaCaT cells. Our results revealed that, without UVA challenge, Nrf2

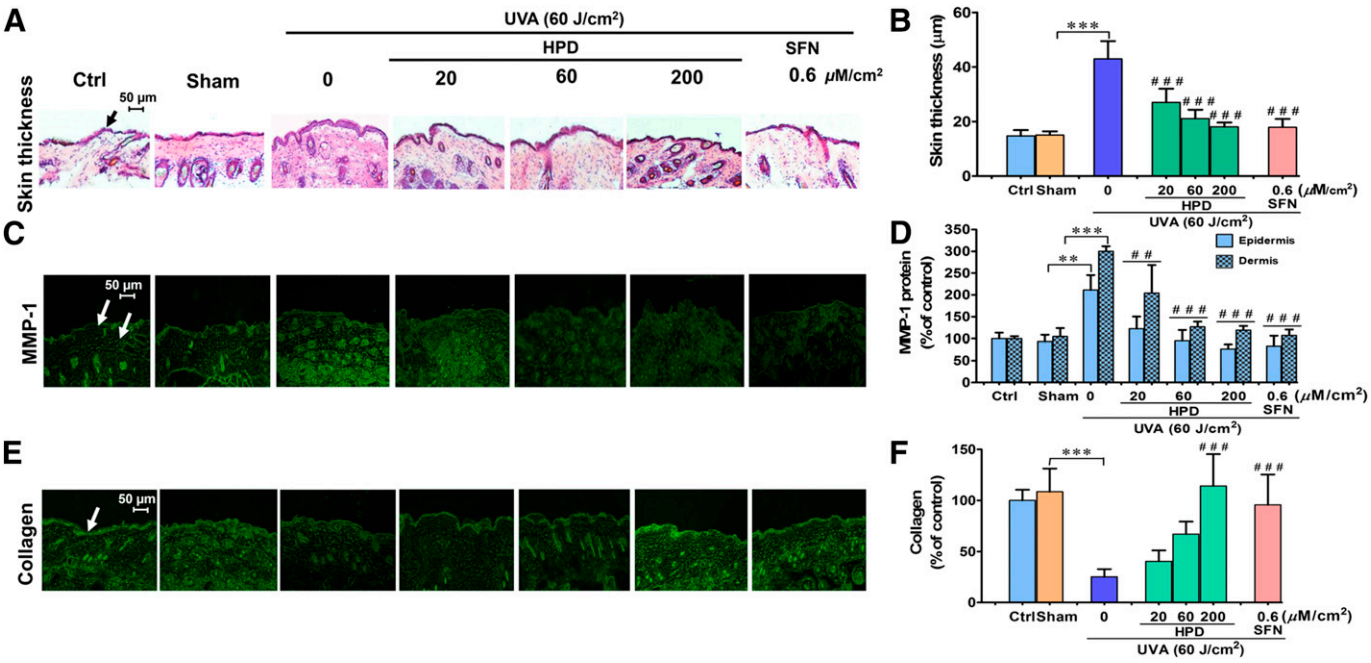

Fig. 4. HPD and SFN alleviate UVA-induced MMP-1 upregulation in vivo. (A) Images of H&E staining for epidermal thickness as indicated by the black arrow. Dorsal skin was pretreated with 20, 60, and 200 μM/cm^2 HPD and 0.6 μM/cm^2 SFN for 1 hour prior to each UVA irradiation (10 J/cm^2/session three times per week for 2 weeks; a total dose of 60 J/cm^2). The skin was collected at 1 hour following the last UV exposure. H&E samples were collected using 20× objectives as scale bar = 50 μm. Images of immunofluorescence staining for MMP-1 protein (C) in mouse epidermis and dermis and for collagen (E) in mouse dermis skin. Dorsal skin was pretreated with test compounds for 1 hour prior to each UVA irradiation and was collected at 24 hours following the last UV exposure. The epidermal thickness (B) and levels of MMP-1 protein (D) and collagen (F) modulated by topical application of HPD and SFN prior to UVA exposure were quantified by ImageJ software. Data were shown as mean ± S.D., $n = 9$. The statistical significance of differences between unirradiated sham control groups and the sham-irradiated groups was evaluated by independent Student's t test. $^{**}P < 0.01$; $^{***}P < 0.001$ versus unirradiated control skin (sham). The statistical significance of differences between irradiated groups pretreated with compounds and the sham-irradiated groups was evaluated by one-way analysis of variance, followed by Dunnett's test. $^{\#\#}P < 0.01$; $^{\#\#\#}P < 0.001$ versus the sham-irradiated groups.

depletion did not affect all parameters studied, including MMP-1 mRNA and activity as well as ROS levels in siNrf2-transfected cells. However, a marked increase in ROS formation was observed in Nrf2-depleted HaCaT cells following UVA challenge, indicating that depletion of Nrf2 may enhance MMP-1 mRNA expression and activity via a ROS-dependent mechanism. Oxidative stress has been reported to mediate activation of MAPKs (including ERK, JNK, and p38) and AP-1 cascades that act as a crucial upstream signaling in controlling transcription of MMPs, mainly MMP-1 in several cell types, including human skin fibroblasts and keratinocytes (Jung et al., 2014; Kim et al., 2015). Consistent with results of previous studies (Johansson et al., 2000; Park et al., 2013b), our observations illustrated that MAPK signaling could function as an upstream mediator of MMP-1 in HaCaT cells. We then determined whether MAPK/AP-1 signaling cascades could underlie the protective role of Nrf2 in UVA-induced MMP-1 activity. The results revealed that inhibition of ERK, JNK, and p38 MAPK pathways reverts the unregulation of UVA-mediated MMP-1 under Nrf2 deficiency. ROS-dependent mechanisms could be the cause of UVA-induced MAPK phosphorylation during Nrf2 depletion because treatment of HaCaT cells with H_2O_2 led to activation of MAPK signaling cascades in the Nrf2-depleted HaCaT cells after UVA irradiation, together with the elevated ROS level.

We also investigated the photoprotective effects of HPD and SFN, a well-known Nrf2 inducer, on UVA-induced MMP-1 expression and collagen degradation, a hallmark of skin aging, in association with phosphorylated levels of MAPKs (ERK, JNK, and p38) and the AP-1 components, c-Jun and c-Fos, under the in vivo setting. Several studies have suggested that phytochemicals that can activate Nrf2 provide pharmacological effects against photodamage and photocarcinogenesis of the skin (Benedict et al., 2012; Tao et al., 2013), although the underlying molecular mechanisms were still unknown. HPD is a potentially active component in Thai traditional medicine for treatment of skin disorders and for skin care. Additionally, HPD has been demonstrated to possess anti-inflammatory activities via activation of Nrf2 (Pluemsamran et al., 2013; Akram et al., 2015). SFN was used in this study because it is a well-known Nrf2 inducer and has been shown to protect against UV-induced oxidative damage and apoptosis in ex vivo human skin (Kleszczyński et al., 2013) and against UVB-mediated cytotoxicity in HaCaT cells and fibroblasts (Talalay et al., 2007; Wagner et al., 2010). Moreover, topical administration of SFN-containing broccoli sprout extracts inhibited skin carcinogenesis induced by UVB in SKH1 hairless mice, which genetically modified by SKH1(a MEK signaling) and hr(hairless) gene (Dinkova-Kostova et al., 2006) and SFN applied topically to murine skin protected against UVB-mediated inflammation and sunburn reaction (Saw et al., 2011). However, the photoprotective effects of HPD and SFN on UVA-induced MMP-1 upregulation and collagen depletion in association with activation of MAPK/AP-1 signaling have not been reported. In our in vivo study, following repetitive UVA irradiation at 10 J/cm^2/session three times per week for 2 weeks (the total dose of 60 J/cm^2), consistent with our previous in vitro observations (Chaiprasongsuk et al., 2016), UVA was shown to cause a transient decrease in Nrf2 nuclear translocation at 1 hour postirradiation and in protein

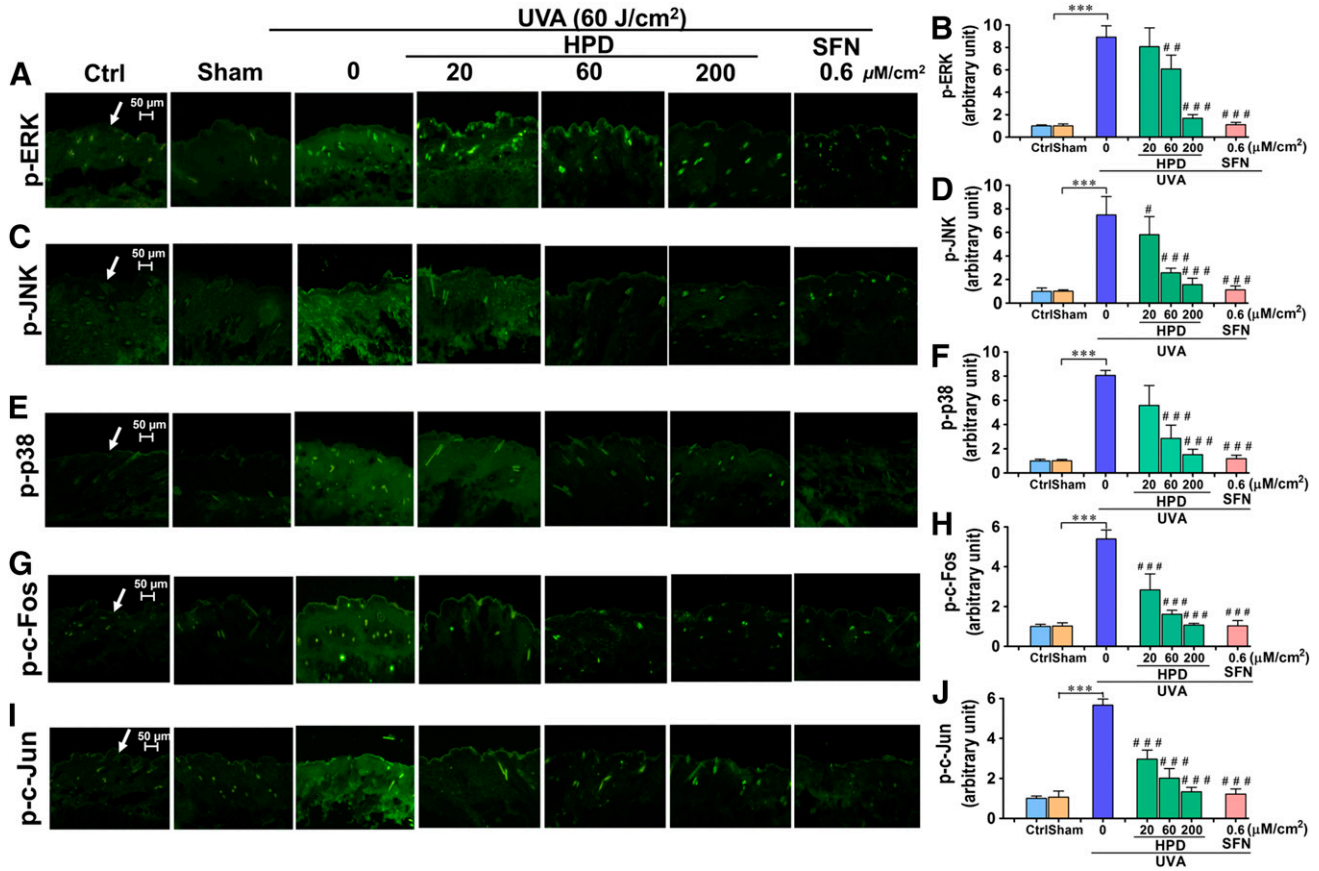

Fig. 5. HPD and SFN suppressed phosphorylation of MAPK/AP-1 signaling cascades after UVA irradiation of the skin. Immunofluorescence image of phosphorylated ERK (A), JNK (C), p38 (E), c-Fos (G), and c-Jun (I) in mouse epidermis. Dorsal skin was pretreated with 20, 60, and 200 μM/cm^2 HPD and 0.6 μM/cm^2 SFN for 1 hour prior to each UVA irradiation (10 J/cm^2/session three times per week for 2 weeks; a total dose of 60 J/cm^2). The skin was collected at 15 minutes following the last UV exposure. Levels of phosphorylated ERK (B), JNK (D), p38 (F), c-Fos (H), and c-Jun (J) modulated by topical application of HPD and SFN prior to UVA exposure were quantified by ImageJ software. Data were shown as mean ± S.D., $n = 9$. The statistical significance of differences between unirradiated sham control groups and the sham-irradiated groups was evaluated by independent Student's t test. ***$P < 0.001$ versus unirradiated control skin (sham). The statistical significance of differences between irradiated groups pretreated with compounds and the sham-irradiated groups was evaluated by one-way analysis of variance, followed by Dunnett's test. #$P < 0.05$; ##$P < 0.01$; ###$P < 0.001$ versus the sham-irradiated groups.

levels of its target antioxidants (GCLC, GST, and NQO1) at 6 hours postirradiation in the epidermis of mouse skin, although a restoration of protein expressions of nuclear Nrf2 and its target antioxidants was observed at later time points. Both HPD and SFN were demonstrated to induce Nrf2 nuclear accumulation and protein expressions of GCLC, GST, and NQO1 in UVA-irradiated mouse skin, indicating that test compounds possessed Nrf2-activating properties correlated with their abilities to reduce oxidative DNA damage induced by UVA. Furthermore, our in vivo study confirmed that SFN acted as a direct Nrf2 activator because topical treatment with SFN alone without UVA irradiation could promote Nrf2 nuclear translocation and its target antioxidant expressions in mice skin. In contrast, HPD was more likely an indirect activator of Nrf2 because treatment with HPD alone without UVA irradiation did not affect the nuclear Nrf2 level or its target proteins, although HPD could induce Nrf2-mediated antioxidant enzymes in mice skin with UVA irradiation.

We further determined the antiphotoaging effects of HPD and SFN on mice skin, which were repeatedly irradiated with UVA irradiation (10 J/cm^2) three times weekly for 2 weeks. Topical treatment of mice with HPD (20–200 μM/cm^2) or SFN (0.6 μM/cm^2) for 1 hour prior to each irradiation reduced epidermal thickness, commonly observed as a defense mechanism to guard against photodamage, at 1 hour after the final irradiation of repetitive irradiation (the total dose of 60 J/cm^2). In addition, both test compounds abrogated MMP-1 protein and retained collagen levels at 24 hours in mice skin after the final irradiation. Previous studies using cultured human keratinocytes and dermal fibroblasts have suggested that UVA irradiation plays a role in upregulation of MMP-1 involved in photodamage through oxidative stress (Rushworth et al., 2011; Pluemsamran et al., 2012; Chaiprasongsuk et al., 2016). Transcription of MMP-1, a AP-1 target gene, can be stimulated by phosphorylation of c-Jun and c-Fos, which cooperate to regulate AP-1–dependent gene transcription, upon activation of upstream MAPKs (including ERK, JNK, and p38) (Frigo et al., 2004; Ho et al., 2011). Our observations suggest that HPD and SFN, having abilities to activate Nrf2, suppressed UVA-induced photoaging involving MMP-1 induction and collagen destruction in mouse skin. To further explore signal transduction mechanisms, this study revealed relevance of the in vivo to in vitro findings that HPD and SFN could reverse the UVA-dependent increase of phosphorylation of ERK, JNK, p38, c-Jun, and c-Fos in mouse skin, suggesting that both test compounds serving as Nrf2-activating compounds

can protect skin against UVA-mediated MMP-1 induction and collagen depletion possibly through inactivation of MAPK/AP-1 signaling pathways. Previous studies reported redox-dependent anti-inflammatory actions of natural compounds and herbal extracts possessing antioxidant properties in various disease models, including photodamaged skin (Mantena and Katiyar, 2006; Liu et al., 2011; Saw et al., 2011). Glycyrrhizic acid, a component of licorice, was shown to suppress UVB-mediated oxidative damage of cellular compartments, including mitochondria and endoplasmic reticulum, apoptosis, and activation of MAPK pathway in human skin fibroblasts (Farrukh et al., 2015). Youngiasides A and C suppressed UVB-induced MMP-1 production possibly through Nrf2-mediated antioxidant response in association with down-regulation of MAPK and AP-1 signalings in HaCaT cells (Kim et al., 2015). Suppression of heme oxygenase-1 reversed the protective effect of celastrol on inflammatory responses by downregulation of JNK MAPK/AP-1 signaling pathways in astrocytes (Youn et al., 2014). Moreover, Nrf2 depletion enhanced activation of MAPKs, including JNK, ERK, and p38, and induction of c-Fos in osteoclast differentiation induced by inflammatory cascades (Hyeon et al., 2013). Therefore, MAPK/AP-1 signaling involved in the photoaging process could be redox regulated via Nrf2-dependent antioxidant responses.

Taken together, our observations demonstrate for the first time that, upon oxidative insults induced by UVA irradiation, Nrf2 deficiency resulted in hyperactivation of MMP-1 activity through activation of MAPK/AP-1 signaling. Both HPD and SFN, potent Nrf2 activators, were shown to have photoprotective effects against repetitive UVA, reducing MMP-1 induction and restoring collagen formation, possibly via inactivation of MAPK/AP-1 signaling pathways. In this respect, indirect or direct targeting of Nrf2-dependent antioxidant response may represent a promising pharmacological strategy for prevention and inhibition of skin photoaging.

Acknowledgments

The authors are grateful to Dr. Naravat Poungvarin, Department of Clinical Pathology, and Assistant Professor Chantacha Sitticharoon, Department of Physiology, Faculty of Medicine, Siriraj Hospital, Mahidol University, for technical assistance and advice. The technical assistance and advice provided by Siriraj Laboratory for Systems Pharmacology is also acknowledged.

Authorship Contributions

Participated in research design: Panich.

Conducted experiments: Chaiprasongsuk, Lohakul, Soontrapa.

Performed data analysis: Chaiprasongsuk, Sampattavanich, Panich.

Wrote or contributed to the writing of the manuscript: Panich, Chaiprasongsuk, Sampattavanich, Akarasereenont.

References

Akram M, Syed AS, Kim KA, Lee JS, Chang SY, Kim CY, and Bae ON (2015) Heme oxygenase 1-mediated novel anti-inflammatory activities of Salvia plebeia and its active components. *J Ethnopharmacol* **174**:322–330.

Avci P, Sadasivam M, Gupta A, De Melo WC, Huang YY, Yin R, Chandran R, Kumar R, Otufowora A, Nyame T, et al. (2013) Animal models of skin disease for drug discovery. *Expert Opin Drug Discov* **8**:331–355.

Baumann L (2007) Skin ageing and its treatment. *J Pathol* **211**:241–251.

Benedict AL, Knatko EV, and Dinkova-Kostova AT (2012) The indirect antioxidant sulforaphane protects against thiopurine-mediated photooxidative stress. *Carcinogenesis* **33**:2457–2466.

Boddupalli S, Mein JR, Lakkanna S, and James DR (2012) Induction of phase 2 antioxidant enzymes by broccoli sulforaphane: perspectives in maintaining the antioxidant activity of vitamins A, C, and E. *Front Genet* **3**:7.

Brugè F, Tiano L, Astolfi P, Emanuelli M, and Damiani E (2014) Prevention of UVA-induced oxidative damage in human dermal fibroblasts by new UV filters, assessed using a novel in vitro experimental system. *PLoS One* **9**:e83401.

Chaiprasongsuk A, Onkoksoong T, Pluemsamran T, Limsaengurai S, and Panich U (2016) Photoprotection by dietary phenolics against melanogenesis induced by UVA through Nrf2-dependent antioxidant responses. *Redox Biol* **8**:79–90.

Chao SW, Su MY, Chiou LC, Chen LC, Chang CI, and Huang WJ (2015) Total synthesis of hispidulin and the structural basis for its inhibition of proto-oncogene kinase Pim-1. *J Nat Prod* **78**:1969–1976.

Dinkova-Kostova AT, Jenkins SN, Fahey JW, Ye L, Wehage SL, Liby KT, Stephenson KK, Wade KL, and Talalay P (2006) Protection against UV-light-induced skin carcinogenesis in SKH-1 high-risk mice by sulforaphane-containing broccoli sprout extracts. *Cancer Lett* **240**:243–252.

Endo H, Watanabe T, Sugioka Y, Niioka M, Inagaki Y, and Okazaki I (2009) Activation of two distinct MAPK pathways governs constitutive expression of matrix metalloproteinase-1 in human pancreatic cancer cell lines. *Int J Oncol* **35**: 1237–1245.

Farrukh MR, Nissar UA, Kaiser PJ, Afnan Q, Sharma PR, Bhushan S, and Tasduq SA (2015) Glycyrrhizic acid (GA) inhibits reactive oxygen species mediated photodamage by blocking ER stress and MAPK pathway in UV-B irradiated human skin fibroblasts. *J Photochem Photobiol B* **148**:351–357.

Fisher GJ, Kang S, Varani J, Bata-Csorgo Z, Wan Y, Datta S, and Voorhees JJ (2002) Mechanisms of photoaging and chronological skin aging. *Arch Dermatol* **138**: 1462–1470.

Frigo DE, Tang Y, Beckman BS, Scandurro AB, Alam J, Burow ME, and McLachlan JA (2004) Mechanism of AP-1-mediated gene expression by select organochlorines through the p38 MAPK pathway. *Carcinogenesis* **25**:249–261.

Frohlich DA, McCabe MT, Arnold RS, and Day ML (2008) The role of Nrf2 in increased reactive oxygen species and DNA damage in prostate tumorigenesis. *Oncogene* **27**:4353–4362.

Gao MQ, Guo SB, Chen XH, Du W, and Wang CB (2007) Molecular mechanisms of polypeptide from Chlamys farreri protecting HaCaT cells from apoptosis induced by UVA plus UVB. *Acta Pharmacol Sin* **28**:1007–1014.

Gawronska-Kozak B, Grabowska A, Kur-Piotrowska A, and Kopcewicz M (2016) Foxn1 transcription factor regulates wound healing of skin through promoting epithelial-mesenchymal transition. *PLoS One* **11**:e0150635.

Gęgotek A and Skrzydlewska E (2015) The role of transcription factor Nrf2 in skin cells metabolism. *Arch Dermatol Res* **307**:385–396.

Grimbaldeston MA, Geczy CL, Tedla N, Finlay-Jones JJ, and Hart PH (2003) S100A8 induction in keratinocytes by ultraviolet A irradiation is dependent on reactive oxygen intermediates. *J Invest Dermatol* **121**:1168–1174.

Ham SA, Kang ES, Lee H, Hwang JS, Yoo T, Paek KS, Park C, Kim JH, Lim DS, and Seo HG (2013) PPARδ inhibits UVB-induced secretion of MMP-1 through MKP-7-mediated suppression of JNK signaling. *J Invest Dermatol* **133**:2593–2600.

Ho BY, Wu YM, Chang KJ, and Pan TM (2011) Dimerumic acid inhibits SW620 cell invasion by attenuating H_2O_2-mediated MMP-7 expression via JNK/C-Jun and ERK/C-Fos activation in an AP-1-dependent manner. *Int J Biol Sci* **7**:869–880.

Hwang KA, Yi BR, and Choi KC (2011a) Molecular mechanisms and in vivo mouse models of skin aging associated with dermal matrix alterations. *Lab Anim Res* **27**: 1–8.

Hwang YP, Oh KN, Yun HJ, and Jeong HG (2011b) The flavonoids apigenin and luteolin suppress ultraviolet A-induced matrix metalloproteinase-1 expression via MAPKs and AP-1-dependent signaling in HaCaT cells. *J Dermatol Sci* **61**:23–31.

Hyeon S, Lee H, Yang Y, and Jeong W (2013) Nrf2 deficiency induces oxidative stress and promotes RANKL-induced osteoclast differentiation. *Free Radic Biol Med* **65**: 789–799.

Johansson N, Ala-aho R, Uitto V, Grénman R, Fusenig NE, López-Otín C, and Kähäri VM (2000) Expression of collagenase-3 (MMP-13) and collagenase-1 (MMP-1) by transformed keratinocytes is dependent on the activity of p38 mitogen-activated protein kinase. *J Cell Sci* **113**:227–235.

Jung YR, Kim DH, Kim SR, An HJ, Lee EK, Tanaka T, Kim ND, Yokozawa T, Park JN, and Chung HY (2014) Anti-wrinkle effect of magnesium lithospermate B from Salvia miltiorrhiza BUNGE: inhibition of MMPs via NF-κB signaling. *PLoS One* **9**: e102689.

Kammeyer A and Luiten RM (2015) Oxidation events and skin aging. *Ageing Res Rev* **21**:16–29.

Kang KA, Zhang R, Piao MJ, Ko DO, Wang ZH, Lee K, Kim BJ, Shin T, Park JW, Lee NH, et al. (2008) Inhibitory effects of triphlorethol-A on MMP-1 induced by oxidative stress in human keratinocytes via ERK and AP-1 inhibition. *J Toxicol Environ Health A* **71**:992–999.

Kim M, Park YG, Lee HJ, Lim SJ, and Nho CW (2015) Youngiasides A and C isolated from Youngia denticulatum inhibit UVB-Induced MMP expression and promote type I procollagen production via repression of MAPK/AP-1/NF-κB and activation of AMPK/Nrf2 in HaCaT cells and human dermal fibroblasts. *J Agric Food Chem* **63**:5428–5438.

Kleszczyński K, Ernst IM, Wagner AE, Kruse N, Zillikens D, Rimbach G, and Fischer TW (2013) Sulforaphane and phenylethyl isothiocyanate protect human skin against UVR-induced oxidative stress and apoptosis: role of Nrf2-dependent gene expression and antioxidant enzymes. *Pharmacol Res* **78**:28–40.

Kook SH, Jang YS, and Lee JC (2011) Involvement of JNK-AP-1 and ERK-NF-κB signaling in tension-stimulated expression of type I collagen and MMP-1 in human periodontal ligament fibroblasts. *J Appl Physiol (1985)* **111**:1575–1583.

Kwak JY, Seok JK, Suh HJ, Choi YH, Hong SS, Kim DS, and Boo YC (2016) Anti-melanogenic effects of luteolin 7-sulfate isolated from Phyllospadix iwatensis Makino. *Br J Dermatol* **175**:501–511.

Liu Y, Chan F, Sun H, Yan J, Fan D, Zhao D, An J, and Zhou D (2011) Resveratrol protects human keratinocytes HaCaT cells from UVA-induced oxidative stress damage by downregulating Keap1 expression. *Eur J Pharmacol* **650**:130–137.

López-Camarillo C, Ocampo EA, Casamichana ML, Pérez-Plasencia C, Alvarez-Sánchez E, and Marchat LA (2012) Protein kinases and transcription factors

activation in response to UV-radiation of skin: implications for carcinogenesis. *Int J Mol Sci* **13**:142–172.
Mantena SK and Katiyar SK (2006) Grape seed proanthocyanidins inhibit UV-radiation-induced oxidative stress and activation of MAPK and NF-kappaB signaling in human epidermal keratinocytes. *Free Radic Biol Med* **40**:1603–1614.
McCloy RA, Rogers S, Caldon CE, Lorca T, Castro A, and Burgess A (2014) Partial inhibition of Cdk1 in G 2 phase overrides the SAC and decouples mitotic events. *Cell Cycle* **13**:1400–1412.
Noursadeghi M, Tsang J, Haustein T, Miller RF, Chain BM, and Katz DR (2008) Quantitative imaging assay for NF-kappaB nuclear translocation in primary human macrophages. *J Immunol Methods* **329**:194–200.
Panich U, Sittithumcharee G, Rathviboon N, and Jirawatnotai S (2016) Ultraviolet radiation-induced skin aging: the role of DNA damage and oxidative stress in epidermal stem cell damage mediated skin aging. *Stem Cells Int* **2016**:7370642.
Park G, Kim HG, Sim Y, Sung SH, and Oh MS (2013a) Sauchinone, a lignan from Saururus chinensis, protects human skin keratinocytes against ultraviolet B-induced photoaging by regulating the oxidative defense system. *Biol Pharm Bull* **36**:1134–1139.
Park M, Han J, Lee CS, Soo BH, Lim KM, and Ha H (2013b) Carnosic acid, a phenolic diterpene from rosemary, prevents UV-induced expression of matrix metalloproteinases in human skin fibroblasts and keratinocytes. *Exp Dermatol* **22**: 336–341.
Pluemsamran T, Onkoksoong T, and Panich U (2012) Caffeic acid and ferulic acid inhibit UVA-induced matrix metalloproteinase-1 through regulation of antioxidant defense system in keratinocyte HaCaT cells. *Photochem Photobiol* **88**:961–968.
Pluemsamran T, Tripatara P, Phadungrakwittaya R, Akarasereenont P, Laohapand T, and Panich U (2013) Redox mechanisms of AVS022, an oriental polyherbal formula, and its component herbs in protection against induction of matrix metalloproteinase-1 in UVA-irradiated keratinocyte HaCaT cells. *Evid Based Complement Alternat Med* **2013**:739473.
Rushworth SA, Shah S, and MacEwan DJ (2011) TNF mediates the sustained activation of Nrf2 in human monocytes. *J Immunol* **187**:702–707.
Ryu J, Park SJ, Kim IH, Choi YH, and Nam TJ (2014) Protective effect of porphyra-334 on UVA-induced photoaging in human skin fibroblasts. *Int J Mol Med* **34**: 796–803.
Saw CL, Huang MT, Liu Y, Khor TO, Conney AH, and Kong AN (2011) Impact of Nrf2 on UVB-induced skin inflammation/photoprotection and photoprotective effect of sulforaphane. *Mol Carcinog* **50**:479–486.
Sayama A, Soushin T, Okada T, Doi K, and Nakayama H (2010) Morphological and biochemical changes during aging and photoaging of the skin of C57BL/6J mice. *J Toxicol Pathol* **23**:133–139.
Seo WY, Goh AR, Ju SM, Song HY, Kwon DJ, Jun JG, Kim BC, Choi SY, and Park J (2011) Celastrol induces expression of heme oxygenase-1 through ROS/Nrf2/ARE signaling in the HaCaT cells. *Biochem Biophys Res Commun* **407**:535–540.
Shimada E, Aida K, Sugawara T, and Hirata T (2011) Inhibitory effect of topical maize glucosylceramide on skin photoaging in UVA-irradiated hairless mice. *J Oleo Sci* **60**:321–325.
Talalay P, Fahey JW, Healy ZR, Wehage SL, Benedict AL, Min C, and Dinkova-Kostova AT (2007) Sulforaphane mobilizes cellular defenses that protect skin against damage by UV radiation. *Proc Natl Acad Sci USA* **104**:17500–17505.
Tao S, Justiniano R, Zhang DD, and Wondrak GT (2013) The Nrf2-inducers tanshinone I and dihydrotanshinone protect human skin cells and reconstructed human skin against solar simulated UV. *Redox Biol* **1**:532–541.
Thitilertdecha P, Guy RH, and Rowan MG (2014) Characterisation of polyphenolic compounds in Clerodendrum petasites S. Moore and their potential for topical delivery through the skin. *J Ethnopharmacol* **154**:400–407.
Wagner AE, Ernst I, Iori R, Desel C, and Rimbach G (2010) Sulforaphane but not ascorbigen, indole-3-carbinole and ascorbic acid activates the transcription factor Nrf2 and induces phase-2 and antioxidant enzymes in human keratinocytes in culture. *Exp Dermatol* **19**:137–144.
Wondrak GT, Cabello CM, Villeneuve NF, Zhang S, Ley S, Li Y, Sun Z, and Zhang DD (2008) Cinnamoyl-based Nrf2-activators targeting human skin cell photooxidative stress. *Free Radic Biol Med* **45**:385–395.
Youn GS, Kwon DJ, Ju SM, Rhim H, Bae YS, Choi SY, and Park J (2014) Celastrol ameliorates HIV-1 Tat-induced inflammatory responses via NF-kappaB and AP-1 inhibition and heme oxygenase-1 induction in astrocytes. *Toxicol Appl Pharmacol* **280**:42–52.

Address correspondence to: Dr. Uraiwan Panich, Department of Pharmacology, Faculty of Medicine Siriraj Hospital, Mahidol University, 2 Prannok Road, Bangkoknoi, Bangkok 10700, Thailand. E-mail: uraiwan.pan@mahidol.ac.th

Activation of Nrf2 reduces UVA-mediated MMP-1 upregulation via MAPK/AP-1 signaling cascades: the photoprotective effects of sulforaphane and hispidulin

Anyamanee Chaiprasongsuk, Jinaphat Lohakul, Kitipong Soontrapa, Somponnat Sampattavanich, Pravit Akarasereenont, Uraiwan Panich

Department of Pharmacology (A.C., J.L., K,S., S.S., P.A.), Center of Applied Thai Traditional Medicine, Faculty of Medicine Siriraj Hospital, Mahidol University, Bangkok 10700, Thailand (P.A.)

Journal of Pharmacology and Experimental Therapeutics

---

*Corresponding author. Address: Department of Pharmacology, Faculty of Medicine Siriraj Hospital, Mahidol University, Bangkok 10700, Thailand. Tel.: +66-(0)2-419-7569; Fax: +66-(0)2-411-5026.

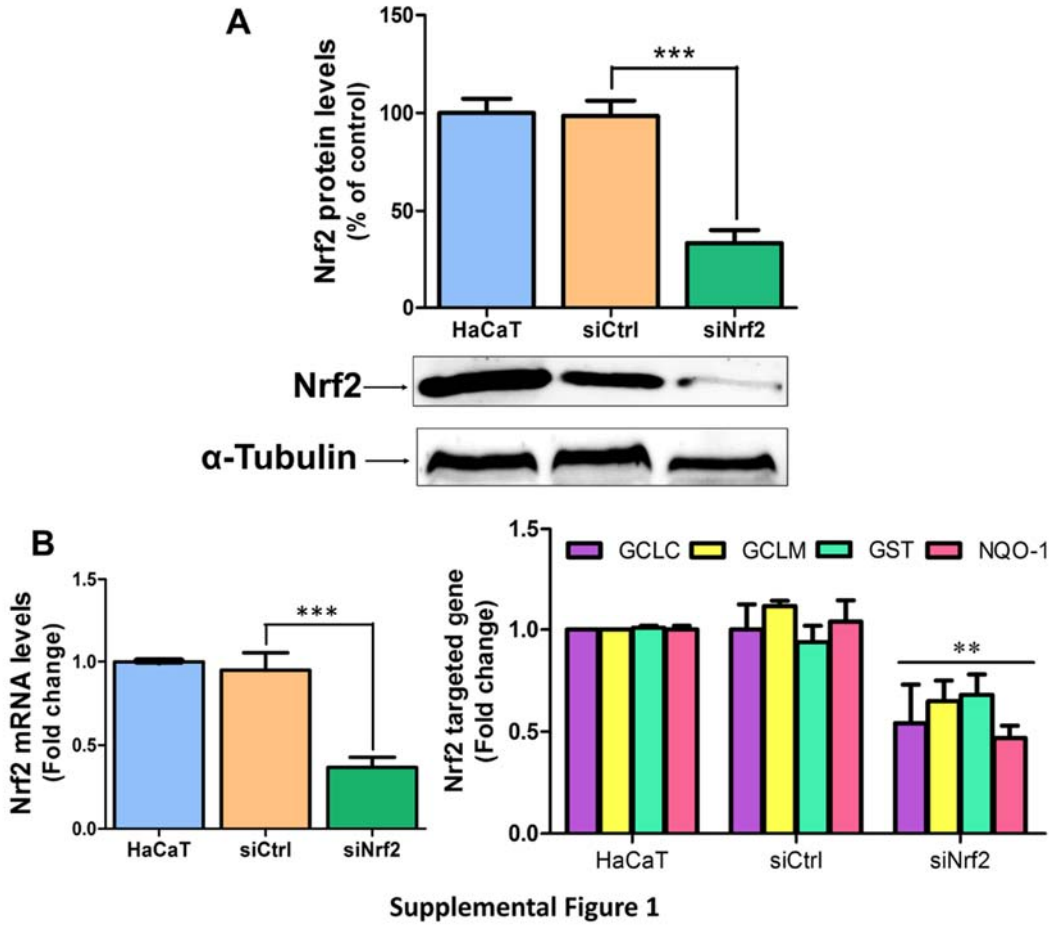

Supplemental Figure 1. The knockdown efficiency of small-interfering RNA-mediated silencing of Nrf2 in HaCaT cells.

Nrf2 protein expression (A) and mRNA expression of Nrf2 and its target genes (GCLC, GCLM, GST and NQO-1) (B) in HaCaT cells transfected with 5 nM of siNrf2 or siCtrl for 48 h. Nrf2 protein levels were detected by Western blot analysis. Data was normalized using α-Tubulin as an internal standard. Nrf2 protein was detected at 68 kDa and α-Tubulin, the loading control, at 50 kDa. mRNA levels were evaluated by real-time RT-PCR. Data was shown as mean ± SD. The statistical significance of differences was evaluated by one-way ANOVA followed by Dunnett's test. ** $P < 0.01$; *** $P < 0.001$ versus untransfected control cells.

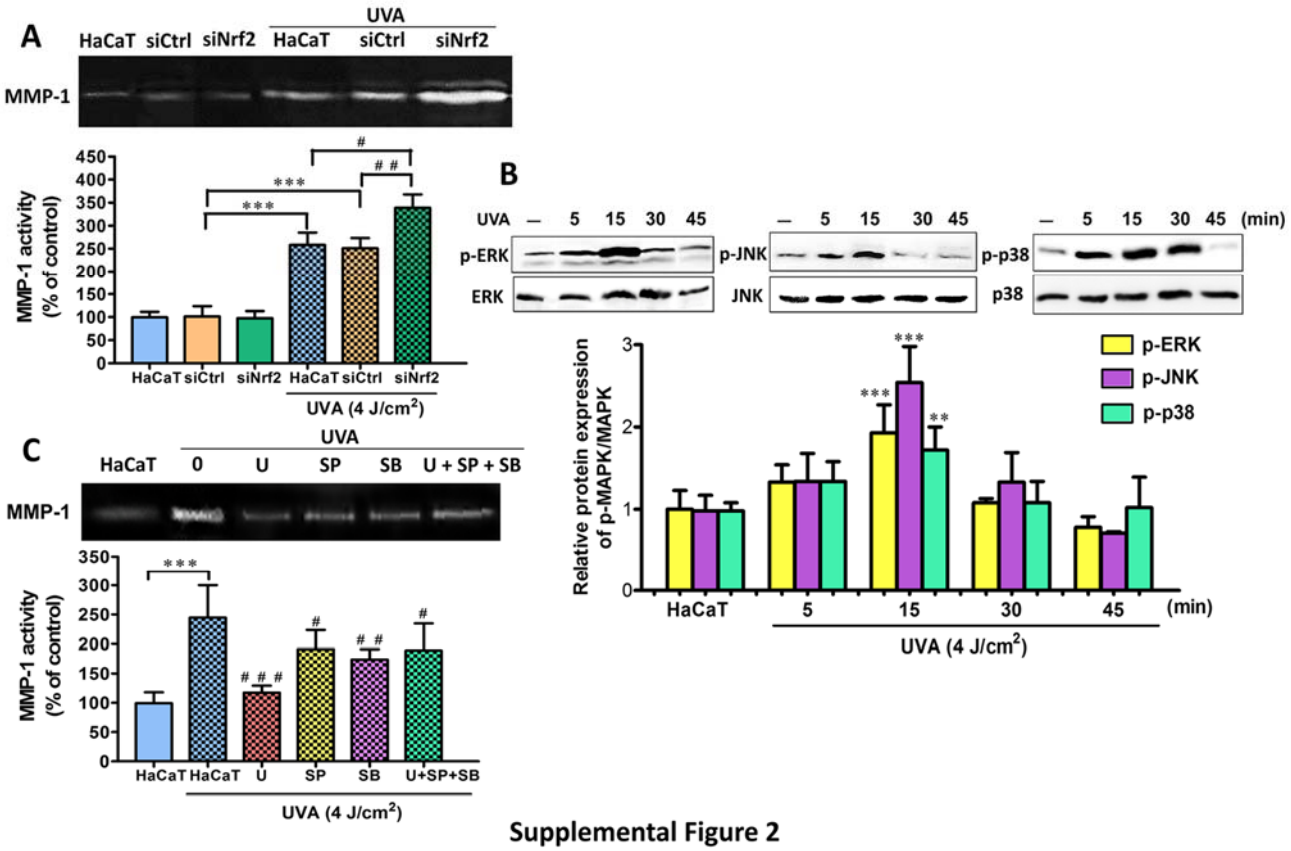

Supplemental Figure 2

Supplemental Figure 2. Nrf2 depletion enhanced UVA-induced MMP-1 activity in association with phosphorylation of ERK, JNK and p38 MAPK in keratinocyte HaCaT cells.

(A) MMP-1 activity in HaCaT cells transfected with siNrf2 or siCtrl for 48 h prior to UVA (4 J/cm^2) irradiation. The cells were harvested at 24 h post-irradiation for detection of MMP-1 activity by zymography. Data was expressed as mean ± SD. The statistical significance of differences was evaluated by one-way ANOVA followed by Dunnett's test. *** $P < 0.001$ versus siCtrl-transfected cells without UVA irradiation. # $P < 0.05$; ## $P < 0.01$ versus siNrf2-transfected cells irradiated with UVA. (B) Time-dependent effects of UVA (4 J/cm^2) irradiation on phosphorylation of MAPKs in HaCaT cells. Phosphorylated-MAPK protein levels were measured at 5, 15, 30, 45 min following irradiation. The statistical significance of differences between non-irradiated controls and the UVA-irradiated groups was evaluated by one-way

ANOVA followed by Dunnett's test. *$P < 0.05$; **$P < 0.01$; ***$P < 0.001$ versus unirradiated control cells. (C) MMP-1 activity in HaCaT cells pre-treated with 1 μM of U0126, SP600125 and SB203580 for 1 h prior to UVA (4 J/cm^2) exposure. The statistical significance of differences between non-irradiated controls and the UVA-irradiated groups was evaluated by independent Student's *t*-test. *** $P < 0.001$ versus unirradiated control cells. The statistical significance of differences between non-irradiated groups pre-treated with compounds and the irradiated control groups was evaluated by one-way ANOVA followed by Dunnett's test. # $P < 0.05$; ## $P < 0.01$; ### $P < 0.001$ versus UVA-irradiated cells.

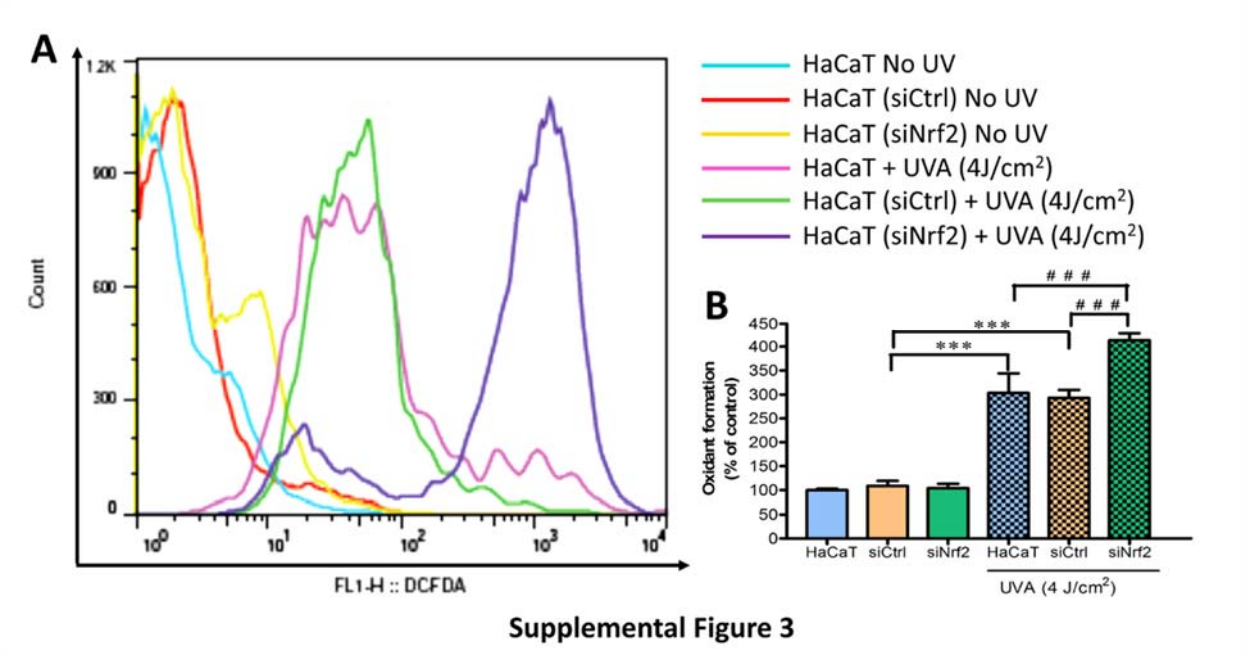

Supplemental Figure 3. Depletion of Nrf2 increased ROS levels in UVA-irradiated HaCaT cells.

(A) ROS levels were detected in HaCaT cells transfected with siNrf2 or siCtrl at 1 h following UVA (4 J/cm^2) irradiation. (B) Quantitative analysis of oxidant formation. Determination of DCFDA was performed by flow cytometry and data was expressed as a percentage of control (100%, non-irradiated and untransfected cells). The statistical significance of differences was evaluated by one-way ANOVA followed by Dunnett's test. *** $P < 0.001$ versus siCtrl-transfected cells without UVA irradiation. ### $P < 0.001$ versus siNrf2-transfected cells irradiated with UVA.

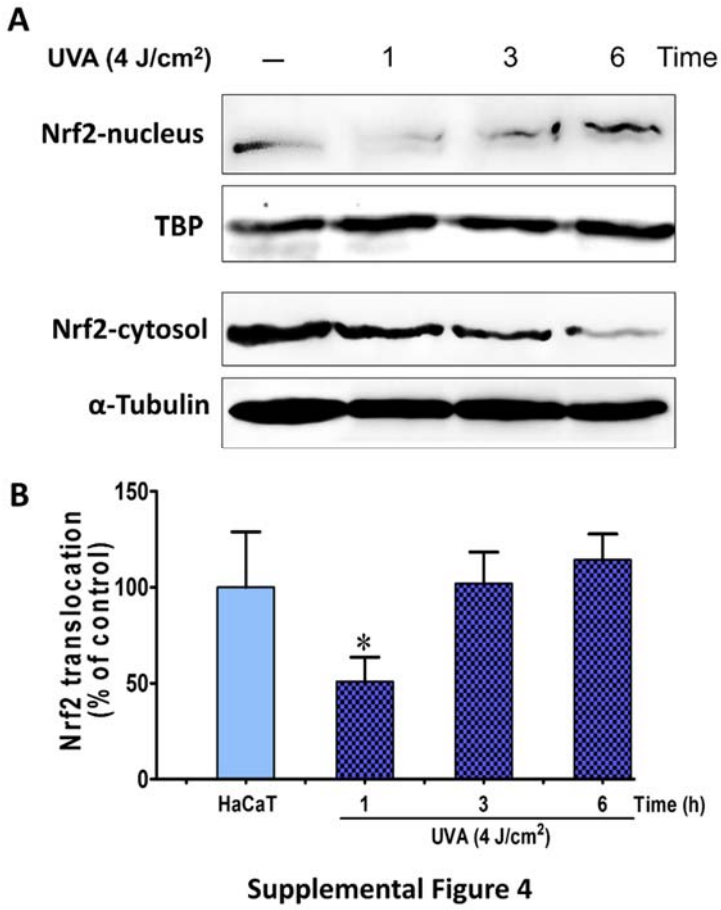

Supplemental Figure 4. The time-dependent changes in Nrf2 nuclear accumulation in HaCaT cells exposed to UVA irradiation.

(A) Time-dependent effects of UVA (4 J/cm^2) on Nrf2 nuclear translocation in HaCaT cells harvested at 1, 3 and 6 h after UVA exposure. Western blot was performed to determine Nrf2 nuclear translocation. Nrf2 was detected at 68 kDa, TATA-binding protein (TBP), the loading control for nuclear protein, at 37 kDa and and α-Tubulin, the loading control for cytosol protein, at 50 kDa. (B) Quantitative analysis of Nrf2 nuclear translocation (% of control) expressed as mean ± SD. The statistical significance of differences was evaluated by one-way ANOVA followed by Dunnett's test. * $P < 0.05$ versus unirradiated control cells.

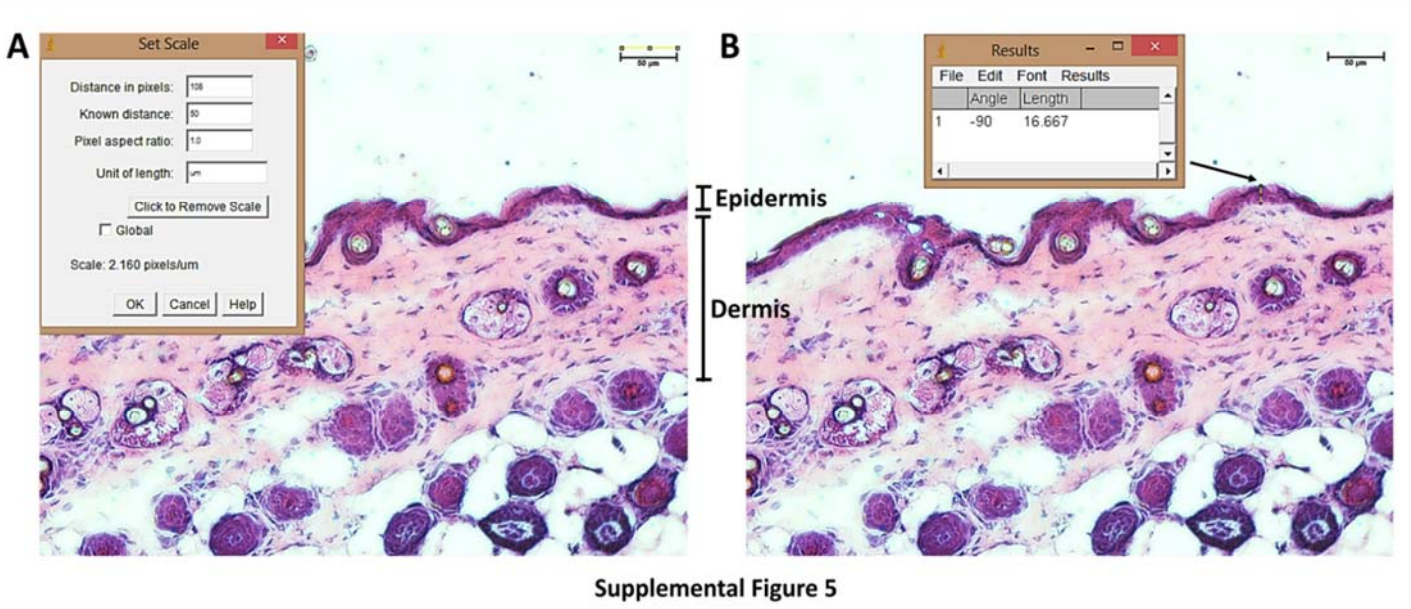

Supplemental Figure 5

Supplemental Figure 5. Epidermal thickness analysis of images by image J software.

(A) The distance in pixels (108 pixels) were defined from scale bar (50 μm) indicated by inverted fluorescent microscope with camera (Ti-S Intensilight Ri1 NIS-D) as shown in yellow line. (B) Drawing the yellow line in epidermis and measured by ImageJ. The data were generated length in μm unit.

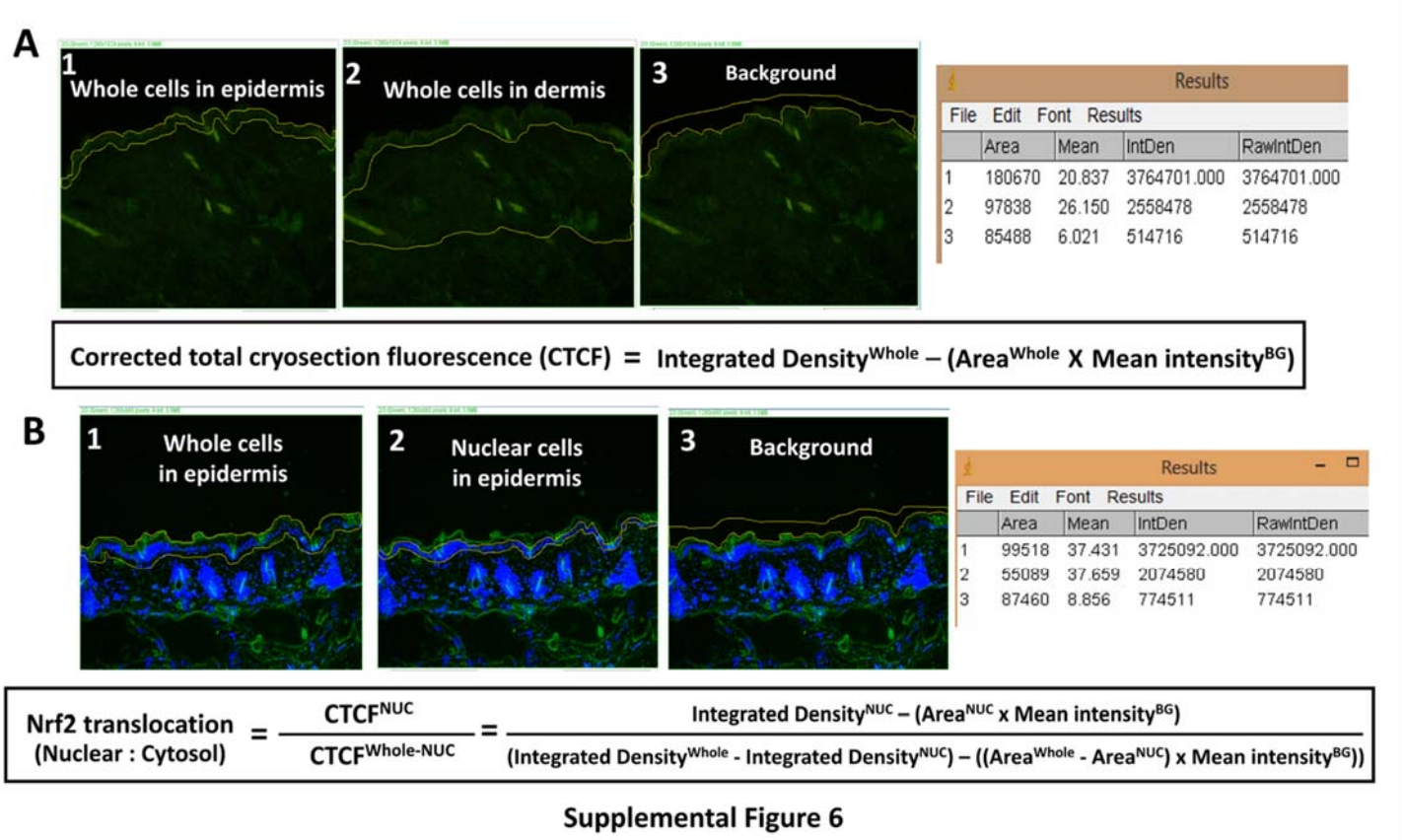

Supplemental Figure 6

Supplemental Figure 6. Fluorescence intensity analysis of images by image J software. (A) To determined protein markers, images of FITC staining were split into green and blue channels. Whole cells in epidermis (1) and whole cells in dermis (2) and background (3) were segmented as shown in yellow lines. Images from 3 rounds of FITC staining were quantified in pixel intensity at green channel. The intensity data measured by ImageJ were generated area, mean intensity and integrated density of yellow line selection. The corrected total cryosection fluorescence (CTCF) = integrated density – (area of selected cell × mean fluorescence of background readings) was calculated as shown in equations. (B) To determined Nrf2 translocation, images of FITC/DAPI staining were split into green and blue channels. Whole cells (1) and nuclear cells (2) in epidermis and background (3) were segmented as shown in yellow lines. Nuclear masks were generated from DAPI staining. Epidermis area was located and confirmed by the pathologist followed by morphological image (Supplementary Fig. S5). Images from 3 rounds of FITC staining were quantified in pixel intensity at green

channel. The intensity data measured by ImageJ were generated area and integrated density of yellow line selection. The ratio of nuclear and cytosolic Nrf2 was calculated as shown in equations.

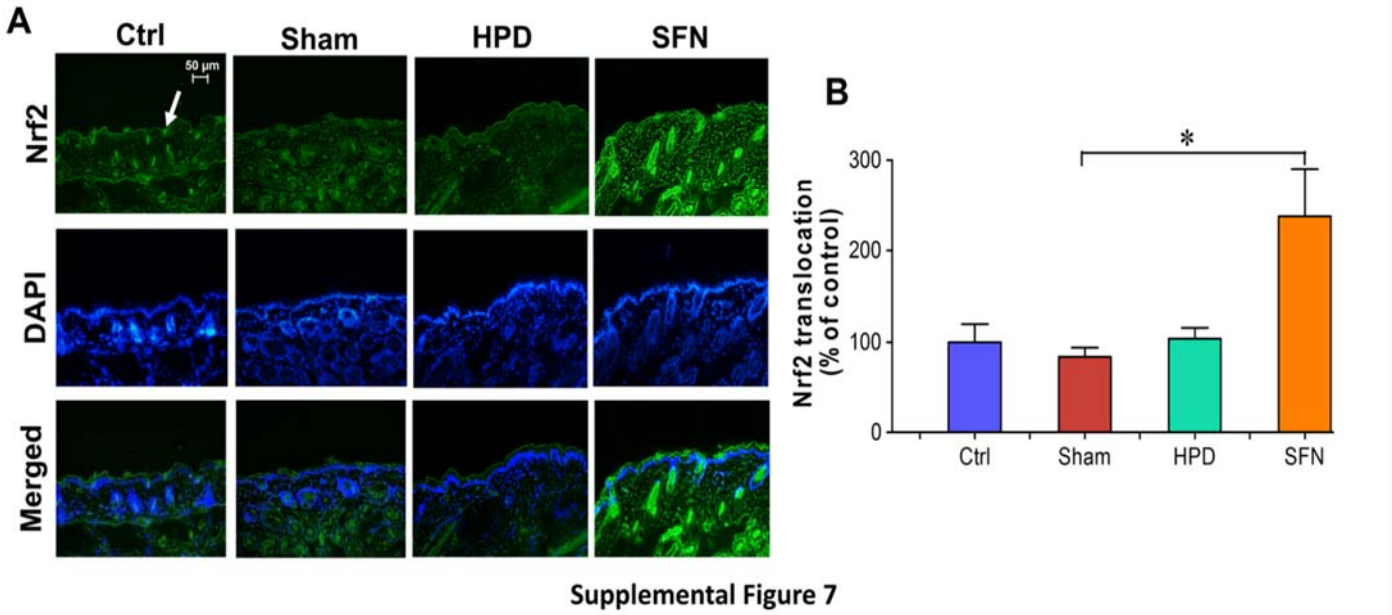

Supplemental Figure 7

Supplemental Figure 7. The effect of hispidulin (HPD) and sulforaphane (SFN) on Nrf2 nuclear localization in unirradiated control skin.

(A) Mice were topically treated over the dorsal skin with 20 µl of vehicle [ethanol:acetone (1:1, v/v)] as sham group, HPD at the highest dose used in this study (200 μM/cm^2) and SFN (0.6 μM /cm^2) for 1 h (3 times a week for 2 weeks) without UVA exposure. The skin was collected at 1 h following the last treatment. Immunofluorescence staining using anti-Nrf2 antibody and FITC-conjugated secondary antibody was performed to determine Nrf2 nuclear localization indicating Nrf2 activation in mouse epidermis. As shown with the white arrow, FITC-conjugated secondary antibody staining indicated location of Nrf2 (green) by anti-Nrf2 antibody. DAPI staining indicated the location of the nucleus (blue) and the merged image indicated the nuclear localization of Nrf2. (B) Levels of nuclear/cytosolic Nrf2 in mouse epidermis topically treated with HPD or SFN alone were quantified by ImageJ software and were expressed as mean ± SD, $n = 9$. The statistical significance of differences between sham control groups and the compound-treated groups was evaluated by one-way ANOVA followed by Dunnett's test. * $P < 0.05$ versus untreated control skin.

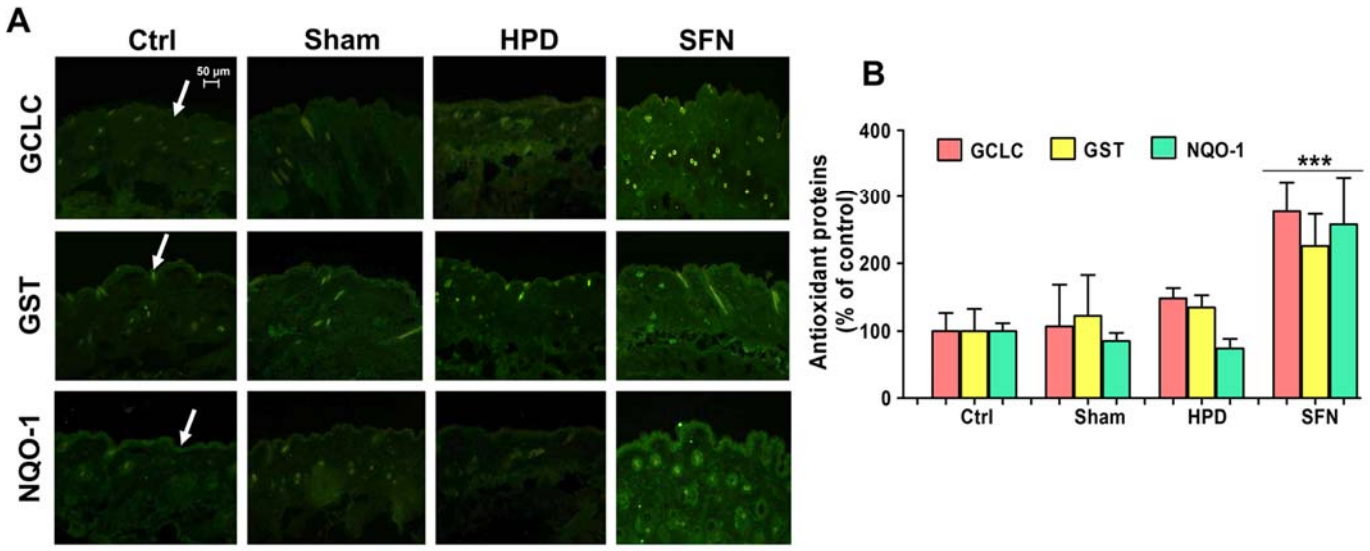

Supplemental Figure 8

Supplemental Figure 8. The effect of hispidulin (HPD) and sulforaphane (SFN) on Nrf2 targeted proteins in unirradiated control skin.

(A) Mice were topically treated over the dorsal skin with 20 µl of vehicle [ethanol:acetone (1:1, v/v)] as sham group, HPD at the highest dose used in this study (200 μM/cm^2) and SFN (0.6 μM /cm^2) for 1 h (3 times a week for 2 weeks) without UVA exposure. The skin was collected at 6 h following the last treatment. Immunofluorescence staining was performed to determine Nrf2 targeted proteins (GCLC, GST and NQO-1) indicated with the white arrow. (B) Protein levels of GCLC, GST and NQO-1 in mouse skin topically treated with HPD or SFN alone were quantified by ImageJ software. Data was shown as mean ± SD, n = 9. The statistical significance of differences between sham control groups and the compound-treated groups was evaluated by one-way ANOVA followed by Dunnett's test. *** $P < 0.001$ versus sham control skin.

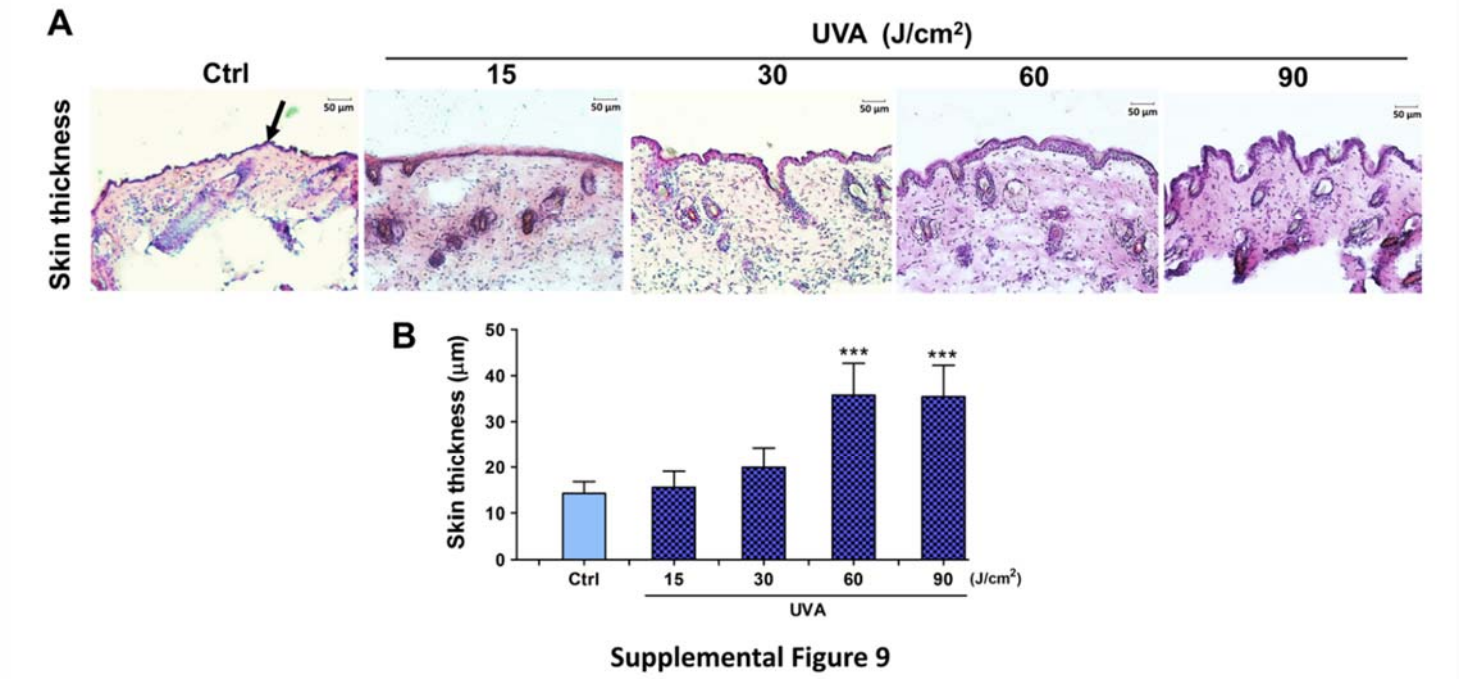

Supplemental Figure 9. Dose-dependent effects of UVA irradiation on the epidermal thickness of mouse skin.

(A) Images of H&E staining for epidermal thickness as indicated by the black arrow. Mouse dorsal skin was irradiated with different doses of UVA irradiation (15, 30, 60 and 90 J/cm^2) and was collected at 1 h after the last irradiation. (B) The epidermal thickness of mouse skin were quantified by ImageJ software. Data was shown as mean ± SD, n = 9. The statistical significance of differences between unirradiated control groups and the UVA-irradiated groups was evaluated by one-way ANOVA followed by Dunnett's test. *** $P < 0.001$ versus unirradiated control skin.

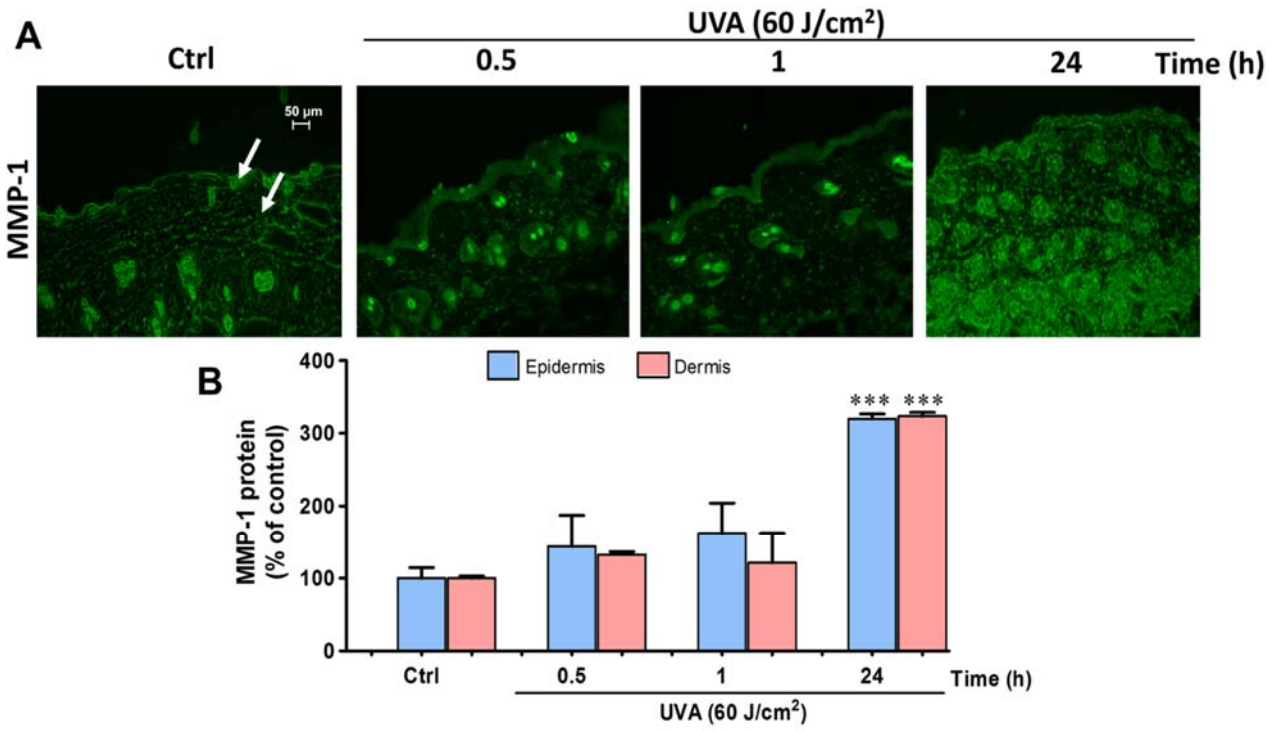

Supplemental Figure 10

Supplemental Figure 10. The effects of UVA (60 J/cm^2) irradiation on MMP-1 expression in mouse skin.

(A) Images of immunofluorescence staining for MMP-1 protein in mouse epidermis and dermis. Mouse skin was collected at 0.5, 1 and 24 h after the final irradiation with UVA (10 J/cm^2/session 3 times a week for 2 weeks; a total dose of 60 J/cm^2). (B) MMP-1 protein expression in mouse epidermis and dermis was quantified by ImageJ software. Data was shown as mean ± SD, $n = 9$. The statistical significance of differences between unirradiated control groups and the UVA-irradiated groups was evaluated by one-way ANOVA followed by Dunnett's test. *** $P < 0.001$ versus unirradiated control skin.